

Fas Promotes T Helper 17 Cell Differentiation and Inhibits T Helper 1 Cell Development by Binding and Sequestering Transcription Factor STAT1

Highlights

- Fas promotes the *in vivo* pathogenicity of T helper 17 cells
- Fas promotes the stability of T helper 17 cells by preventing STAT1 activation
- Fas regulates the STAT1 versus STAT3 balance by binding and sequestering STAT1
- Fas is a cell-intrinsic regulator of competing T helper cell differentiation programs

Authors

Gerd Meyer zu Horste,
Dariusz Przybylski,
Markus A. Schramm, ...
Raymond Sobel, Aviv Regev,
Vijay K. Kuchroo

Correspondence

aregev@broadinstitute.org (A.R.),
vkuchroo@evergrande.hms.
harvard.edu (V.K.K.)

In Brief

Fas is a well-known death receptor that can also mediate non-apoptotic functions. Meyer zu Horste et al. demonstrate that Fas promotes the stability and pathogenicity of T helper 17 cells by sequestering and inhibiting the activation of STAT1 and regulating the availability of opposing STAT1 and STAT3.



Fas Promotes T Helper 17 Cell Differentiation and Inhibits T Helper 1 Cell Development by Binding and Sequestering Transcription Factor STAT1

Gerd Meyer zu Horste,^{1,2,3} Dariusz Przybylski,^{4,6} Markus A. Schramm,^{1,2,6} Chao Wang,^{1,2} Alexandra Schnell,^{1,2} Youjin Lee,^{1,2} Raymond Sobel,⁵ Aviv Regev,^{4,*} and Vijay K. Kuchroo^{1,2,4,7,*}

¹Evergrande Center for Immunologic Diseases, Harvard Medical School and Brigham and Women's Hospital, Boston, MA, USA

²Ann Romney Center for Neurologic Diseases, Brigham and Women's Hospital, Boston, MA, USA

³Department of Neurology, University Hospital Münster, Münster, Germany

⁴Broad Institute of MIT and Harvard, Cambridge, MA, USA

⁵Palo Alto Veteran's Administration Health Care System and Department of Pathology, Stanford University School of Medicine, Stanford, CA, USA

⁶These authors contributed equally

⁷Lead Contact

*Correspondence: aregev@broadinstitute.org (A.R.), vkuchroo@evergrande.hms.harvard.edu (V.K.K.)

<https://doi.org/10.1016/j.immuni.2018.03.008>

SUMMARY

The death receptor Fas removes activated lymphocytes through apoptosis. Previous transcriptional profiling predicted that Fas positively regulates interleukin-17 (IL-17)-producing T helper 17 (Th17) cells. Here, we demonstrate that Fas promoted the generation and stability of Th17 cells and prevented their differentiation into Th1 cells. Mice with T-cell- and Th17-cell-specific deletion of Fas were protected from induced autoimmunity, and Th17 cell differentiation and stability were impaired. Fas-deficient Th17 cells instead developed a Th1-cell-like transcriptional profile, which a new algorithm predicted to depend on STAT1. Experimentally, Fas indeed bound and sequestered STAT1, and Fas deficiency enhanced IL-6-induced STAT1 activation and nuclear translocation, whereas deficiency of STAT1 reversed the transcriptional changes induced by Fas deficiency. Thus, our computational and experimental approach identified Fas as a regulator of the Th17-to-Th1 cell balance by controlling the availability of opposing STAT1 and STAT3 to have a direct impact on autoimmunity.

INTRODUCTION

Interleukin-17 (IL-17)-producing T helper 17 (Th17) cells have been identified as a distinct lineage of CD4⁺ T helper (Th) cells producing IL-17A and IL-17F. They are critical drivers of autoimmune tissue inflammation in experimental autoimmune encephalomyelitis (EAE) and other autoimmune conditions (Korn et al., 2009). In a recent study, we showed that the Th17 cell differentiation program is regulated through two self-reinforcing and mutually antagonistic modules of positive and negative regula-

tors (Yosef et al., 2013). This model was supported by transcriptional silencing and genetic ablation experiments (Yosef et al., 2013), as well as by chromatin immunoprecipitation sequencing data (Xiao et al., 2014). The positive regulators promote the Th17 cell program while inhibiting the transcriptional programs of other Th cell lineages. This suggests that there is a need not only for positive regulators to push the differentiation into a positive direction but also for concurrent inhibition of opposing differentiation programs to achieve unidirectional T cell differentiation. Other studies also support such a mutually antagonistic design in other Th lineages (O'Shea and Paul, 2010); however, how this is achieved for Th17 cells has not been elucidated.

One of the key positive regulators identified by our model was the prototypic death receptor Fas (Yosef et al., 2013). Our network model predicted that Fas, while promoting Th17 cell differentiation, would also negatively affect the differentiation of other T cell subsets. Initial analysis of *in-vitro*-derived Th17 cells from Fas-deficient (*Fas*^{-/-}) mice showed the predicted reduction in Th17-cell-related gene expression, but the underlying mechanism has not been identified.

Fas has been extensively studied as a trigger of apoptosis in various cell types (Strasser et al., 2009). Indeed, mice carrying a spontaneous Fas mutation (the lymphoproliferation [*lpr*] strain [Watanabe-Fukunaga et al., 1992]) or a Fas ligand (FasL) mutation ([Takahashi et al., 1994]) develop progressive lymphadenopathy and splenomegaly with an accumulation of lymphocytes with an atypical TCR $\alpha\beta^+$ CD4 $^-$ CD8 $^-$ B220 $^+$ phenotype. In addition, Fas signaling has other, non-apoptotic functions, including costimulatory and pro-proliferative effects (Kennedy et al., 1999; Paulsen et al., 2011). T cells deficient in components of the Fas signaling pathway, such as FADD (Walsh et al., 1998) or caspase-8 (Kennedy et al., 1999), have impaired T cell activation and proliferation. Fas activation can thus have opposing outcomes that depend on the cellular context, but whether such non-apoptotic Fas signals also control the differentiation of T cells and specifically Th17 cells has not been elucidated.

In particular, Fas has a suppressive effect on spontaneous systemic autoimmunity but a seemingly paradoxical promoting



effect on induced autoimmunity. Aging *Fas*^{-/-} *lpr* mice spontaneously develop disease signs resembling those of human systemic lupus erythematosus (Cohen and Eisenberg, 1991). Similarly, human patients with loss-of-function or dominant-negative mutations of Fas accumulate lymphocytes and develop various autoimmune phenomena (Holzelova et al., 2004). Fas thus suppresses spontaneous systemic autoimmunity but promotes induced autoimmunity given that *Fas*^{-/-} mice are strongly protected from EAE (Sabelko et al., 1997; Waldner et al., 1997). We hypothesized that our model of opposing and mutually antagonistic gene regulation could provide a starting point for identifying the mechanism that explains these seemingly paradoxical observations.

Here, we demonstrate that Fas promoted the differentiation of Th17 cells and their ability to induce autoimmunity not by affecting apoptosis but rather by promoting their stability and preventing their differentiation into Th1-like cells. We used a computational network analysis on expression profiles from wild-type (WT) and *Fas*^{-/-} cells to nominate STAT1 as the downstream transcription factor (TF) mediating the effects of Fas in Th17 cells. We experimentally validated that Fas indeed directly bound to STAT1 and thus prevented its excessive activation in response to the Th17-cell-differentiating cytokine IL-6 and enhanced Th17 cell stability. Fas thus reciprocally regulates the balance between competing differentiation programs of Th cells by regulating the availability of opposing STAT1 and STAT3. This elucidates an apoptosis-independent function by which Fas controls antagonistic T cell differentiation programs and autoimmunity.

RESULTS

Fas Promotes the Differentiation and Function of Th17 cells

We had previously generated a transcriptional network of differentiating Th17 cells that predicted Fas to be a positive regulator of the Th17 cell differentiation program (Yosef et al., 2013) and a repressor of competing Th cell differentiation programs (Figure 1A).

To test these predictions, we first differentiated CD4⁺ T cells from WT and *Fas*^{-/-} mice *in vitro* by using two Th17-cell-polarizing conditions: (1) TGF-β1 and IL-6 (Bettelli et al., 2006b) and (2) IL-1β, IL-6, and IL-23 (Ghoreschi et al., 2010). *Fas*^{-/-} T cells produced less IL-17A under Th17-cell-culture conditions, whereas interferon-γ (IFN-γ) production under Th1-cell-culture conditions was enhanced both by intracellular cytokine staining (Figure S1A) and by ELISA (Figure S1B). Blocking antibodies against IFN-γ promoted Th17 cell and inhibited Th1 cell differentiation but did not revert the difference between WT and *Fas*^{-/-} cells (Figure S1C), suggesting a propensity to develop Th1 cell responses over Th17 cell responses in the absence of Fas. The differentiation of Th2 cells was also impaired in *Fas*^{-/-} cells (Figure S1D), whereas TGF-β1 FoxP3⁺ induced regulatory T (iTreg) cells were unaffected (Figure S1E). Fas expression was downregulated in the presence of TGF-β1 in differentiating iTreg cells at both the mRNA (Figure S1F) and protein (Figure S1G) levels. Next, we induced EAE in the mice by using myelin oligodendrocyte glycoprotein (MOG) peptide MOG_{35–55}, which requires Th17 cells for its induction (Cua et al., 2003;

Lee et al., 2012). Consistent with previous studies (Waldner et al., 2004), *Fas*^{-/-} mice were almost completely protected from EAE (Figure S2A). Furthermore, *Fas*^{-/-} mice had lower proportions of CD4⁺ T cells producing IL-17 and co-producing IL-17 and IFN-γ and higher proportions of IFN-γ⁺CD4⁺ T cells in their central nervous system (CNS) during EAE than WT mice (Figure S2B). In addition, the antigen-induced generation of IL-17A⁺ cells was reduced and IFN-γ⁺ T cells were increased in draining lymph nodes in *Fas*^{-/-} mice in response to IL-23 stimulation (Figure S2C).

Next, we tested whether Fas deficiency specifically affected Th cells, and for this purpose we generated *Cd4*^{cre}*Fas*^{f/f} mice (STAR Methods). Similar to *Fas*^{-/-} cells, *Cd4*^{cre}*Fas*^{f/f} cells produced less IL-17A under Th17 cell differentiation conditions and more IFN-γ under Th1 cell conditions than those of *Cd4*^{cre}-littermate controls (Figures 1B–1D). *Cd4*^{cre}*Fas*^{f/f} mice were also strongly protected from MOG_{35–55}-induced EAE, as quantified both by clinical scores (Figure 1E) and by the number of inflammatory CNS lesions (Figure 1F). The number of CNS-infiltrating leukocytes was lower (Figure S2D), and CNS-infiltrating CD4⁺ T cells in *Cd4*^{cre}*Fas*^{f/f} mice showed fewer IL-17-producing cells and IL-17- and IFN-γ-producing cells, whereas IFN-γ⁺ cells were increased (Figure 1G and Figure S2D). This indicates that Fas is needed by T cells to promote EAE, enhances Th17 cell differentiation, and represses Th1 cell-responses and thus affects multiple Th lineages.

Next, we tested the function of Fas specifically in Th17 cells by generating *Il17a*^{cre}*Fas*^{f/f} mice, in which Fas was deleted only in IL-17A-producing cells (Hirota et al., 2011). T cells that differentiated from these mice under Th17-cell-polarizing conditions (TGF-β1 and IL-6; or IL-1β, IL-6, and IL-23) showed less IL-17A production than Fas-competent *Il17a*^{cre}*Fas*^{f/f} cells. Production of IFN-γ under Th1-cell-culture conditions was unchanged in *Il17a*^{cre}*Fas*^{f/f} cells (Figures 2A–2C). This validated our genetic targeting because Cre expression and Fas deletion are limited to IL-17A⁺ cells in this mouse line (Hirota et al., 2011), and thus Fas expression in Th1 cells is left intact. *In vivo*, *Il17a*^{cre}*Fas*^{f/f} mice were almost completely protected from EAE by both clinical and histological measures (Figures 2D and 2E). The number of CNS-infiltrating leukocytes was reduced (Figure S2E), and CNS-infiltrating CD4⁺ T cells produced less IL-17A and more IFN-γ than those of *Il17a*^{cre}*Fas*^{f/f} mice (Figure 2F and Figure S2E). Thus, Th17 cells specifically require Fas to promote their differentiation and their *in vivo* function in EAE even when other lineages are Fas competent.

Fas Promotes the Encephalitogenicity of Th17 Cells by Preventing Th17-to-Th1 Cell Conversion

To address Th17 cell stability *in vivo*, we next crossed *Fas*^{-/-} mice to 2D2 mice, which express a MOG_{35–55}-specific T cell receptor (TCR) transgene (Bettelli et al., 2003). Th17 cells that differentiated *in vitro* from *Fas*^{-/-} 2D2 mice induced less severe EAE than WT-2D2 cells after transfer into syngenic C57BL/6 WT hosts, as quantified by clinical and histological measures (Figures 3A and 3B). After transfer, CNS-infiltrating 2D2 T cells, which were identified by the Vα3.2 and Vβ11 chains of the 2D2 TCR, produced less IL-17A and more IFN-γ, whereas co-producers of IL-17A and IFN-γ were unchanged (Figures 3C and 3D) despite comparable pre-transfer

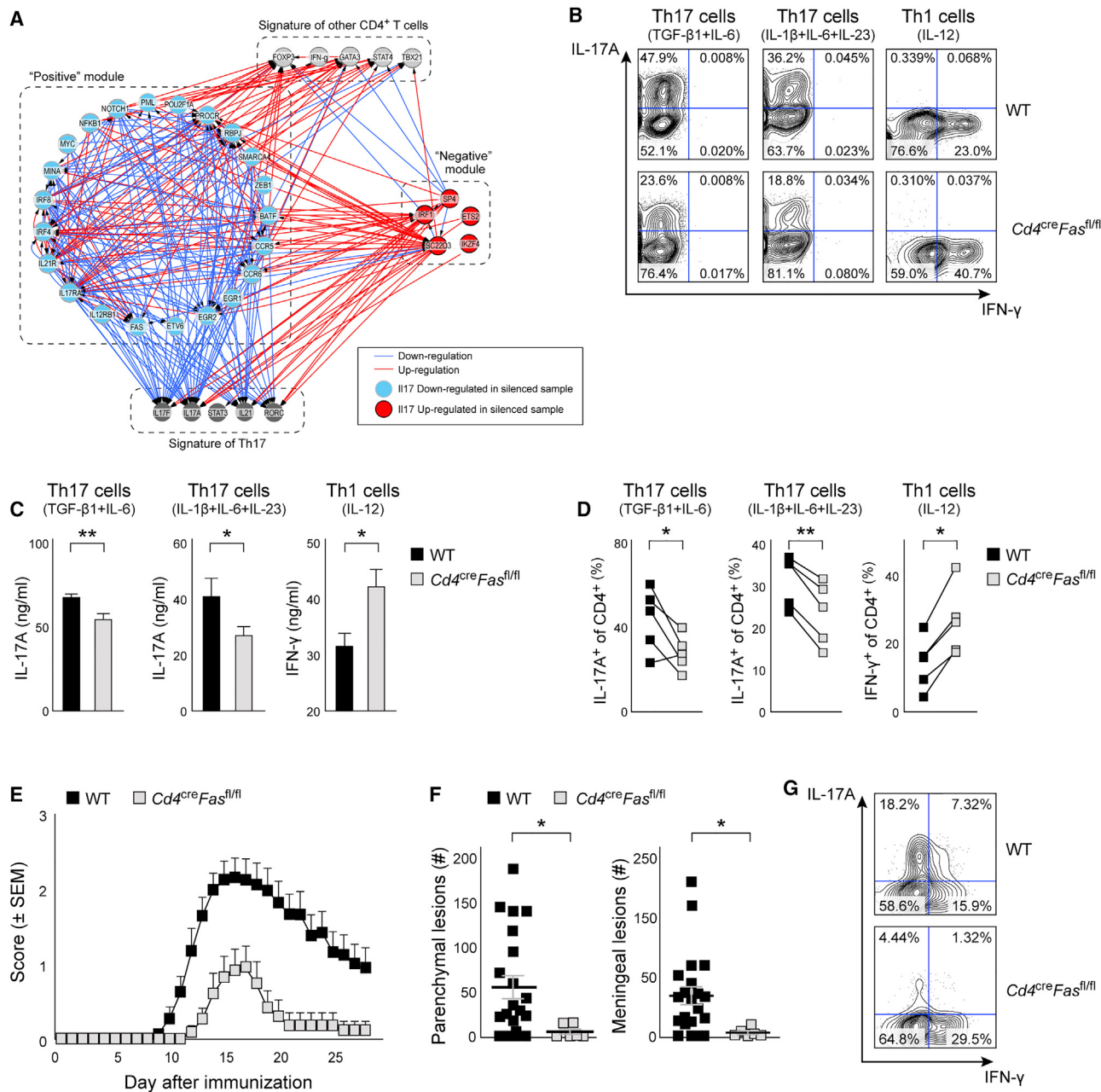


Figure 1. Fas Promotes Th17 Cell Responses and Represses Th1 Cell Differentiation

(A) A Th17 cell transcriptional model adapted from Yosef et al. (2013) consists of two self-reinforcing and mutually antagonistic modules of positive (red nodes) and negative (blue nodes) regulators with opposite effects on Th17 cell signature genes (gray nodes, bottom) and signature genes of other CD4⁺ T cells (gray nodes, top). A blue edge from node A to B indicates that silencing of A downregulates B; a red edge indicates that silencing of A upregulates B. One of five experiments is shown.

(B) Naive CD4⁺CD62L^{high}CD44^{low}CD25⁻ T cells were sorted from *Fas*^{f/f} mice (WT) and *Cd4*^{cre}*Fas*^{f/f} mice, differentiated with (1) TGF- β 1 and IL-6, (2) IL-1 β , IL-6, and IL-23, or (3) IL-12, and analyzed by intracellular cytokine staining after 4 days. One of five experiments is shown.

(C) Supernatants of cultures described in (B) were analyzed by ELISA.

(D) Cytokine-positive cells averaged between technical replicates in individual experiments were quantified.

(E) EAE was induced in WT ($n = 15$) and *Cd4*^{cre}*Fas*^{f/f} ($n = 12$) mice by subcutaneous immunization with 100 μ g of MOG_{35–55} peptide. Mice were monitored daily for EAE signs. Data are summed from three independent experiments.

(F) At day 28 after immunization, inflammatory lesions in the CNS parenchyma and in the meninges were quantified histologically. Data are summed from three independent experiments.

(G) CNS-infiltrating lymphocytes were extracted at the peak of EAE and stained for intracellular cytokines. One of six experiments is shown. Error bars indicate the mean \pm SEM. * $p < 0.05$; ** $p < 0.01$. See also Figure S1.

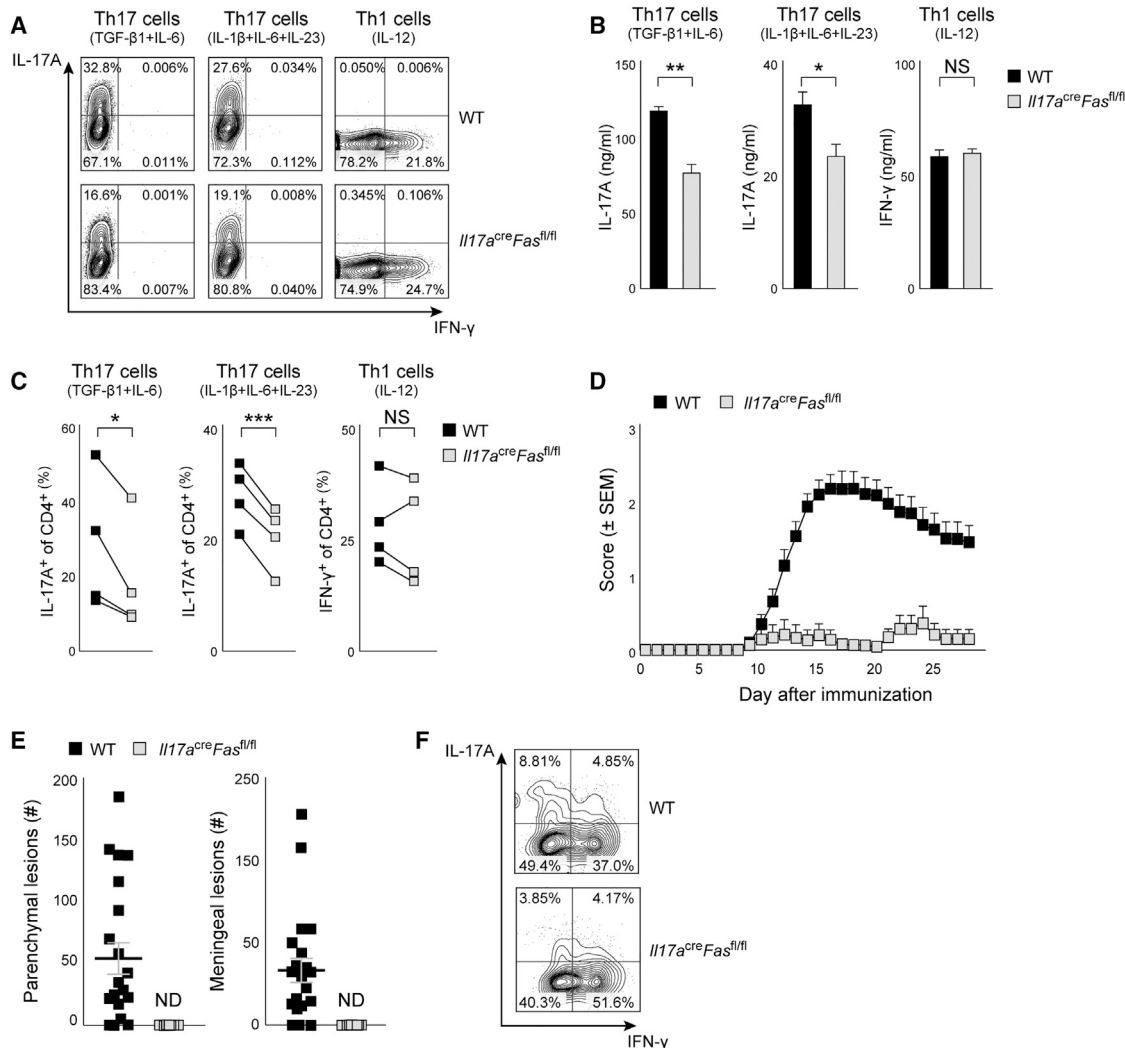


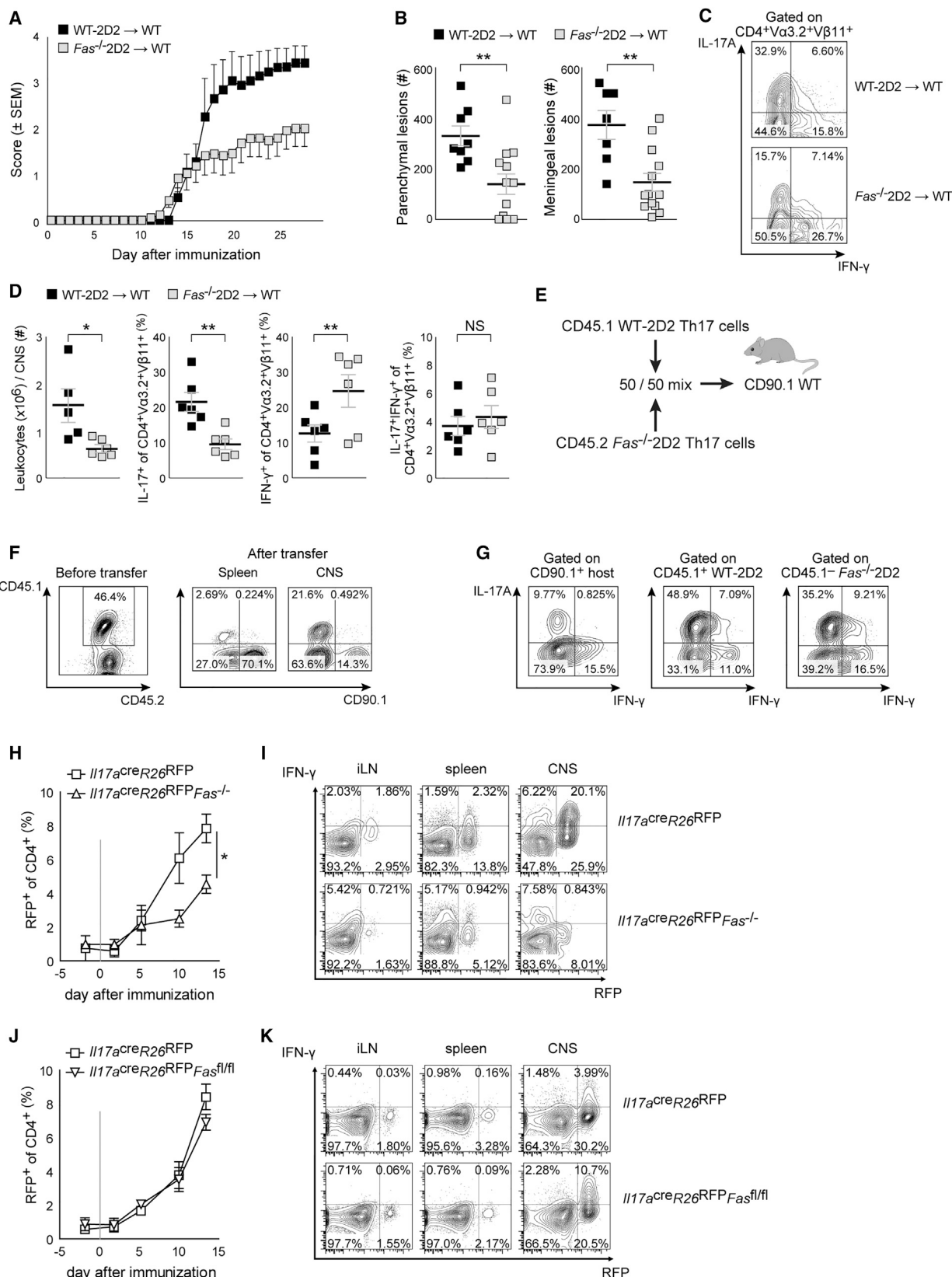
Figure 2. Th17 Cells Require Fas to Promote Their Differentiation and *In Vivo* Function

- (A) Naive CD4⁺CD62L^{high}CD44^{low}CD25⁻ T cells were sorted from WT (*II17a*^{cre}*Fas*^{fl/fl}WT) and *II17a*^{cre}*Fas*^{fl/fl} mice, differentiated with (1) TGF- β 1 and IL-6, (2) IL-1 β , IL-6, and IL-23, or (3) IL-12, and analyzed for intracellular cytokines after 4 days. One of four experiments is shown.
- (B) Supernatants of cell cultures described in (A) were analyzed by ELISA. One of four experiments is shown.
- (C) Cytokine-positive cells were averaged between technical replicates.
- (D) EAE was induced in WT (n = 28) and *II17a*^{cre}*Fas*^{fl/fl} (n = 15) mice by subcutaneous immunization with 100 μ g of MOG_{35–55} peptide. Mice were monitored daily for clinical EAE signs. Data are summed from three experiments.
- (E) At day 28 after immunization, inflammatory lesions in the CNS parenchyma and in the meninges were quantified histologically. Data are summed from three experiments.
- (F) CNS-infiltrating lymphocytes were extracted at the peak of EAE and stained for intracellular cytokines. One of five experiments is shown.
- Error bars indicate the mean \pm SEM. *p < 0.05; ** p < 0.01; ND, not detected; NS, not significant. See also Figure S2.

cytokine production (data not shown). Fewer leukocytes infiltrated the CNS after transfer of *Fas*^{-/-}2D2 donor cells than after transfer of WT-2D2 donor cells (Figure 3D). This indicates that in the absence of Fas, differentiated Th17 cells lose their encephalitogenicity *in vivo* with increased accumulation of Th1-like cells.

We next tested for a T-cell-intrinsic effect of Fas deficiency *in vivo*. We crossed CD45.1 congenic C57BL/6 mice with 2D2 mice (STAR Methods) to transfer EAE with defined antigen specificity (Jäger et al., 2009). We differentiated and transferred a 50/50 mixture of CD4⁺CD45.1⁺ WT-2D2 and CD4⁺CD45.2⁺

Fas^{-/-}2D2 Th17 cells into CD90.1⁺ WT hosts (Figure 3E). After transfer, the proportion of *Fas*^{-/-}2D2 cells (CD4⁺CD45.1⁻CD90.1⁻) was approximately 4-fold greater than that of WT-2D2 cells (CD4⁺CD45.1⁺CD90.1⁻) in the periphery and in the CNS of recipients developing EAE (Figure 3F), consistent with the known enhanced homeostatic expansion of *Fas*^{-/-} T cells *in vivo* (Fortner and Budd, 2005). At the peak of EAE, *Fas*^{-/-}2D2 cells (CD4⁺CD45.1⁻CD90.1⁻) produced less IL-17A and more IFN- γ than WT-2D2 cells (CD4⁺CD45.1⁺CD90.1⁻) (Figure 3G), indicating that the increased propensity for IFN- γ production in the absence of Fas is a cell-intrinsic phenomenon.



(legend on next page)

Of note, we transferred CD4⁺ cells, arguing against a contribution of TCR $\alpha\beta^+$ CD4⁻CD8⁻B220⁺ atypical lymphocytes in these experiments. Furthermore, Fas^{-/-}2D2 Th17 cells expanded relatively more in this mixed-transfer setting (Figure 3F), although they were less pathogenic and produced less IL-17A. This argues for a reduced encephalitogenicity on a per-cell basis and suggests that the influence of Fas deficiency on apoptosis and encephalitogenicity might be independent.

To further delineate the ontogeny of the IFN- γ^+ T cells increased in Fas^{-/-} mice, we next generated *Il17a*^{cre}R26^{RFP} mice crossed to Fas^{-/-} mice (Hirota et al., 2011; Meyer Zu Horste et al., 2016). We found that the continuous accumulation of CD4⁺RFP⁺ cells in the periphery after EAE induction was lower in *Il17a*^{cre}R26^{RFP}Fas^{-/-} mice than in *Il17a*^{cre}R26^{RFP} mice (Figure 3H). Instead, *Il17a*^{cre}R26^{RFP}Fas^{-/-} mice showed an expansion of CD4⁺RFP⁻IFN- γ^+ (i.e., non-Th17) cells both in the periphery and in the CNS at the peak of EAE (Figure 3I and Figure S2F). This indicates that global Fas deficiency in Fas^{-/-} mice impairs the initial lineage commitment of Th17 cells and causes more cells to deviate to a Th1 cell phenotype before RFP expression and Th17 cell differentiation.

We next generated *Il17a*^{cre}R26^{RFP}Fas^{fl/fl} mice to lineage trace Th17 cells while restricting Fas deletion only to IL-17A⁺ cells. The generation of CD4⁺RFP⁺ cells in the periphery after EAE induction was unchanged in *Il17a*^{cre}R26^{RFP}Fas^{fl/fl} mice (Figure 3J). However, IFN- γ^+ cells in *Il17a*^{cre}R26^{RFP}Fas^{fl/fl} mice were increased at the peak of EAE, almost all IFN- γ^+ cells were also RFP⁺, and IFN- γ^+ RFP⁺ cells were 2- to 2.5-fold more abundant in *Il17a*^{cre}R26^{RFP}Fas^{fl/fl} mice (i.e., IFN- γ^+ Th17 cells) than in *Il17a*^{cre}R26^{RFP} mice (Figure 3K and Figure S2G), whereas IL-17A⁺RFP⁺ cells were unchanged (Figure S2G). Th17-cell-restricted Fas deficiency thus causes instability of Th17 cells and their deviation towards a Th1-cell-like phenotype after successful initial commitment to the Th17 cell lineage. This indicates that Fas is persistently needed for maintaining the Th17 cell differentiation program *in vivo*.

We next tested how Fas expression is regulated during T cell differentiation beyond its known induction by TCR engagement and T cell activation (Zheng et al., 2001). In all Th cell subsets, Fas mRNA expression exhibited two early peaks at 4 and 12 hr (these were highest in Th0 cells); then, Fas was continuously upregulated between 48 and 96 hr, and its final expression was highest under Th1 cell conditions and lower under Th0 cell and Th17 cell conditions (Figure S3A). Cell-surface Fas amounts increased in all subsets with culture duration and were highest under Th1 cell conditions and lowest under TGF- β 1 with IL-6-induced Th17 cell conditions (Figure S3B). We next tested whether Th1-cell-inducing IL-12 controls Fas expression in Th17 cells. We found that IL-12 (and TNF- α) enhanced Fas expression on the mRNA and protein levels under IL-1 β , IL-6, and IL-23 conditions, but not under TGF- β 1 and IL-6 conditions (Figures S3C and S3D). IFN- γ and IL-4 had no effect on Fas mRNA expression (data not shown). In accordance with its role in activation-induced cell death, Fas is thus upregulated by activation in all Th cell lineages and is strongly upregulated by Th1-cell-inducing cytokines. Induction of Fas by IL-12 could form an inhibitory feedback loop to limit excessive Th1 cell differentiation.

Caspase Inhibition or Deficiency Does Not Replicate the Fas-Deficiency Phenotype

To address the role of apoptosis in the Th17 cell phenotype in Fas^{-/-} cells, we measured hallmarks of apoptosis during *in vitro* T cell differentiation. Apoptosis rates were overall lower under Th17 cell conditions than under Th1 cell conditions and lower in Th17 cells differentiated with TGF- β 1 and IL-6 than in Th17 cells generated with IL-1 β , IL-6, and IL-23 (Figures S3E–S3G). A higher propensity of Th1 cells than Th17 cells for Fas-dependent apoptosis has been described previously (Cencioni et al., 2015) but does not explain the reduced lineage stability triggered by Th17-cell-restricted Fas deletion. Next, we blocked caspase activation during T cell differentiation. We did not

Figure 3. Fas Promotes the Encephalitogenicity and Stability of Th17 Cells

- (A) Naive CD4⁺CD62L^{high}CD44^{low}CD25⁻ T cells were sorted from WT-2D2 and Fas^{-/-}2D2 mice and differentiated with TGF- β 1 and IL-6 followed by IL-23 (STAR Methods). After 7 days, T cells were intravenously injected into WT C57BL/6 recipients. EAE scores were assessed daily. One of three experiments is shown.
 - (B) At day 28 after transfer, inflammatory lesions in the CNS parenchyma and in the meninges were quantified histologically. Data are merged from three independent experiments.
 - (C) CNS-infiltrating lymphocytes from score-matched mice at the peak of EAE were stained for intracellular cytokines. Gating was on live CD4⁺V α 3.2⁺V β 11⁺ cells.
 - (D) CNS-infiltrating leukocytes and the proportion of cytokine-producing CD4⁺V α 3.2⁺V β 11⁺ cells were quantified. Data are merged from three independent experiments.
 - (E) Th17 cells were differentiated *in vitro* from CD45.1⁺ WT-2D2 and CD45.2⁺ Fas^{-/-}2D2 mice, mixed at equal ratios, and injected intravenously into WT CD90.1 recipients. One of three experiments is shown.
 - (F) The relative proportion of CD45.1⁺CD4⁺ and CD90.1⁺CD4⁺ T cells was analyzed by flow cytometry before transfer and after transfer at the peak of EAE. One of three experiments is shown.
 - (G) At the peak of EAE, CNS-infiltrating leukocytes were stained for intracellular cytokines. Gating was on CD4⁺CD45.1⁺CD90.1⁺ host cells (left), CD4⁺CD45.1⁺CD90.1⁺ WT donor cells (middle), or CD4⁺CD45.1⁺CD90.1⁺Fas^{-/-} donor cells (right). Data are merged from two experiments, and one of three experiments is shown.
 - (H) EAE was induced by immunization with 100 μ g of MOG_{35–55} peptide in *Il17a*^{cre}R26^{RFP} (squares; n = 5) and *Il17a*^{cre}R26^{RFP}Fas^{-/-} (triangles; n = 4) mice, and the proportion of RFP⁺CD4⁺ cells was analyzed by flow cytometry in the peripheral blood.
 - (I) At the peak of EAE, leukocytes were extracted from inguinal lymph nodes (iLNs), the spleen, and the CNS of score-matched mice and analyzed for intracellular cytokine production. Data are merged from three experiments, and one of three experiments is shown.
 - (J) The proportion of RFP⁺CD4⁺ cells was analyzed by flow cytometry in the peripheral blood as in (A) in *Il17a*^{cre}R26^{RFP}Fas^{fl/fl}WT (squares; n = 11) and *Il17a*^{cre}R26^{RFP}Fas^{fl/fl} (inverted triangles; n = 7) mice.
 - (K) Leukocytes from iLNs, the spleen, and the CNS of *Il17a*^{cre}R26^{RFP}Fas^{fl/fl}WT and *Il17a*^{cre}R26^{RFP}Fas^{fl/fl} mice were analyzed by intracellular cytokine staining at the peak of EAE as in (I). One of three experiments is shown.
- Error bars indicate the mean \pm SEM. *p < 0.05; **p < 0.01; NS, not significant. See also Figure S3.

observe differences in the production of IL-17A or IFN- γ between WT cells and Th17 or Th1 cell conditions in the presence of caspase-1, -3, or -8 inhibitors (Figures S3H and S3I) or between WT cells and caspase-3-deficient (*Casp3*^{-/-}) or *Fas*^{-/-}/*Casp3*^{-/-} cells (Figure S3J). Thus, inhibiting the canonical death-receptor pathway does not phenocopy *Fas* deficiency, suggesting that apoptosis-independent mechanisms underlie Th17-to-Th1 cell conversion in the absence of *Fas*.

A STAT1-Dependent Program Is Activated in *Fas*^{-/-} Th17 Cells

To identify potential alternative mechanisms by which *Fas* controls Th17 cell differentiation and stability, we performed RNA sequencing (RNA-seq) (STAR Methods). A signature of key Th17-cell-related transcripts (e.g., *I17f*, *I6ra*, and *Rorc*) was significantly downregulated in *Fas*^{-/-} Th17 cells (Cuffdiff p values 9.5×10^{-4} , 2.1×10^{-2} , and 4.8×10^{-2} , respectively; test described in Trapnell et al., 2010), including the Th17 cell signature cytokine *I17a* (Cuffdiff p value $< 5 \times 10^{-5}$, false-discovery rate [FDR] = 0.01; Figure 4A), whereas key Th1-cell-related transcripts and transcripts controlled by IFN signaling (e.g., *Irf1*, *Irf8*, *Tbx21*, *Gbp2*, *Gbp4*, *Gbp5*, and *Tap1*; Figure 4A) were upregulated. Notably, a signature of genes related to IFN- γ signaling was upregulated in *Fas*^{-/-} cells under both Th17 cell differentiation conditions (rank 1 [FDR = 0.051]; Figure 4B) and Th0 cell conditions (rank 3 [FDR = 0.066]; data not shown) in gene-set enrichment analysis (GSEA) (STAR Methods). This suggests that enhanced IFN signaling is involved in the Th1-cell-like transcriptional profile of *Fas*^{-/-}CD4⁺ T cells even under non-polarizing conditions. Testing key transcripts by qPCR confirmed that *I17a* and *Rorc* were significantly reduced and that *Ifng*, *Tbx21*, and *Irf1* were increased in *Fas*^{-/-} Th17 cells (Figure 4C).

To find TFs that were most likely responsible for the *Fas*-deficiency phenotype, we performed an integrative network analysis (STAR Methods). In brief, the analysis aimed to find potential paths from the perturbed receptor (*Fas*) through protein-protein interaction (PPI) to TFs controlling differentially expressed genes by integrating PPI, TF motif binding, and our RNA-seq expression data. Our algorithm computed weighted paths connecting *Fas* with mouse TFs. The network edge weights reflected external evidence supporting PPI. The node weights indicated the probability that the proteins were present in the cells and were computed from the measured average mRNA expression (STAR Methods). The weights of TF nodes also depended on enrichment of DNA-binding motifs and the differential mRNA expression.

We found *Stat1* to have the strongest integrated evidence as both being regulated by *Fas* and being the cause of the observed phenotype (bootstrap p value $< 10^{-3}$; Figure 4D). Additional analyses corroborated this prediction. First, one of the STAT1 DNA-binding motifs was among the eight TF promoter binding motifs that were enriched in the promoters of differentially expressed genes (*Irf1*, *Sp1*, *Atf3*, *Irf7*, *Irf8*, *Stat1*, *Eik1*, and *Irf2*; Table S1). Second, *Stat1* also contributed to the enrichment score of the IFN- γ signaling set in GSEA (Figure 4B), along with that of the TF genes *Irf1*, *Irf8*, and *Sp100*. Third, querying the regulatory modules from our Ontogenet model of mouse hematopoiesis in the Immunological Genome Project (STAR

Methods) implicated *Dtx3l* and *Stat1* as regulators of two of the most significantly enriched expression modules in our dataset (FDR < 0.05). Two of the network paths between *Fas* and STAT1 in our model (Figure 4E) passed through TRADD and FADD, which physically interact with STAT1 (Wang et al., 2000), providing a potential mechanism for *Fas*-dependent regulation of STAT1. *Stat1* itself was not differentially expressed in our RNA-seq dataset obtained at 48 hr, but signaling through STAT proteins occurs rapidly. In a time-course expression analysis, *Stat1* was indeed upregulated in naive *Fas*^{-/-} cells between 0 and 4 hr under Th17 cell differentiation conditions (Figure 4F), which could reflect ongoing self-induction of STAT1 in naive *Fas*^{-/-} cells before sorting. *Irf1*, which is transcriptionally controlled by STAT1 (Kano et al., 2008), was also upregulated in *Fas*^{-/-} Th17 cells, and its peak expression followed *Stat1* expression (Figure 4F). Upregulation of *Stat1* thus precedes that of *Irf1*, *Tbx21*, and *Ifng*, consistent with the notion that STAT1 is the most proximal TF controlled by *Fas* and controls the IFN signaling signature in our dataset. Other members of the STAT protein family were not differentially expressed in our RNA-seq dataset (Figure S4A) or by qPCR (Figure S4B), suggesting a *Stat1*-specific effect of *Fas* deficiency.

Fas Binds STAT1 and Reduces Its Phosphorylation and Nuclear Translocation

We next tested how *Fas* affects the expression and phosphorylation of STAT1. *Fas*^{-/-} naive CD4⁺ T cells contained higher amounts of both total STAT1 and pSTAT1 under baseline conditions and upon activation by IFN- γ (Figure S5A). The increased total STAT1 amounts could reflect self-induction of STAT1 transcription in naive cells. Th17 cell differentiation does not usually involve IFN- γ -dependent signals but essentially requires that IL-6 activate STAT3 (Harris et al., 2007). The amounts of both total STAT1 and pSTAT1 at baseline and after IL-6 stimulation were higher in *Fas*^{-/-} cells than in WT cells according to western blotting (Figure 5A) and flow cytometry (Figure S5B). STAT1 activity depends on the translocation of pSTAT1 to the nucleus. We found that STAT1 nuclear translocation was more frequent in response to IL-6 stimulation in *Fas*^{-/-} CD4⁺ T cells than in WT cells both in nuclear extracts (Figure 5B) and by cell imaging (Figure 5C and Figures S5C and S5D). The absence of β -actin signal in Figure 5B supports the fact that the nuclear fractions were not contaminated by cytoplasmic contents. IL-6 induces and phosphorylates STAT3, which induces Th17 cell differentiation (Harris et al., 2007; Yang et al., 2007). Notably, STAT1 is known to heterodimerize with STAT3 and inhibit STAT3-dependent transcription (Hu and Ivashkiv, 2009; Villarino et al., 2017). Indeed, the nuclear translocation of STAT3 and pSTAT3 was concomitantly less frequent after IL-6 stimulation in *Fas*^{-/-} T cells than in WT cells (Figure 5B and Figures S5C and S5E). Thus, *Fas* deficiency triggers an excessive activation of STAT1 in response to the Th17-cell-inducing cytokine IL-6, which in turn could inhibit the activation of STAT3 and the expression of STAT3-dependent transcripts (e.g., *I17a* and *Rorc*) while promoting the expression of STAT1-dependent transcripts. In accordance, we found that STAT1 overexpression inhibited the STAT3-driven activation of the *I17a* promoter and that this STAT1-dependent cross-inhibition of a known STAT3 target gene was partially reverted by over-expression of *Fas* in promoter activation studies (Figure S5F).

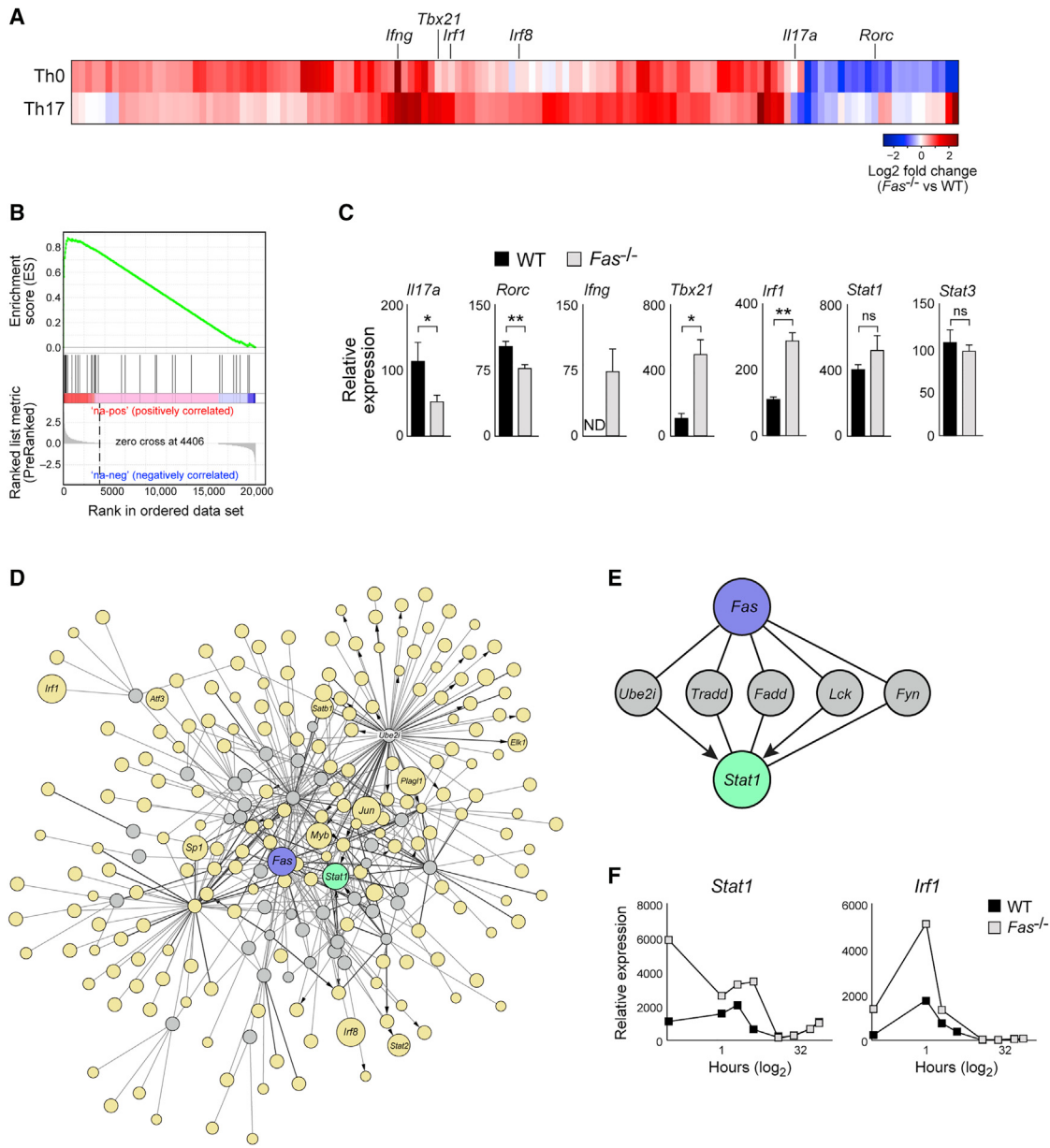


Figure 4. *Fas*^{-/-} Th17 Cells Exhibit a Th1-Cell-like Expression Profile Predicted to be Partially Controlled by STAT1

(A) Naive CD4⁺CD62L^{high}CD44^{low}CD25⁻ T cells from WT and *Fas*^{-/-} mice were differentiated in the presence of TGF-β1 and IL-6 (Th17) or no cytokines (Th0) for 48 hr. Total RNA from the cells was analyzed by RNA-seq (STAR Methods). A heatmap of fold change (log₂) for differentially expressed genes (FDR < 0.05 in Th17 or Th0) is shown.

(B) GSEA identified the most significant enrichment of the IFN-γ signaling pathway. Genes ranked by differential expression (*Fas*^{-/-} versus WT) in Th17 cell conditions were queried against Reactome pathway datasets in MSigDB (STAR Methods).

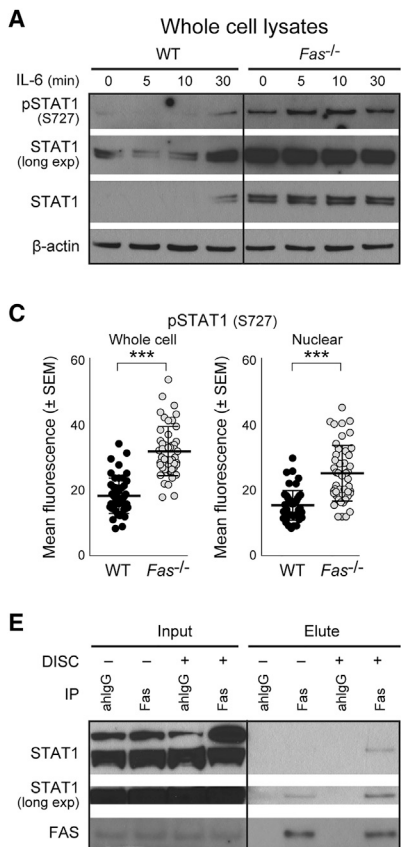
(C) The expression of the selected transcripts was quantified in an independent set of Th17 cell samples (n = 5 per genotype) differentiated with TGF-β1 and IL-6 from naive CD4⁺ T cells for 72 hr by quantitative real-time PCR.

(D) A network algorithm that considered evidence from PPI databases, our RNA-seq expression data, and TF motif enrichment was used for ranking TFs (yellow) that were most likely influenced by Fas (purple). Intermediate nodes (gray) had to be expressed in Th17 or Th0 conditions (FPKM > 3). Arrows indicate directed interactions, such as phosphorylation. STAT1 received the most evidence (green) among network paths containing at most one intermediate node (STAR Methods).

(E) Close up of the PPI network indicating paths from Fas (purple) to STAT1 (green).

(F) Naive T cells were differentiated with TGF-β1 and IL-6 for 72 hr, and RNA was collected at several time points. The expression of *Stat1* and *Irf1* was analyzed by qPCR. The first time point is derived from naive, pre-differentiated cells (i.e., 0 hr) despite the logarithmic scale.

Error bars indicate the mean ± SEM. *p < 0.05; **p < 0.01; ND, not detected; ns, not significant. See also Figure S4.



ice for 15 min (DISC⁻) or stimulated with recombinant multimerized FasL (DISC⁺). Anti-Fas Ab or Armenian hamster IgG was then performed with Protein G Magnetic Beads. Western blotting was performed with the indicated Abs. One of three independent experiments is shown.

***p < 0.005; exp, exposure. See also Figure S5.

Fas thus controls the balance between two opposing STAT proteins.

Next, we tested the PPI predicted in our network model between Fas and STAT1 (Figure 4E). In a mouse T cell line, STAT1 co-immunoprecipitated with Fas after cross-linking of the death-inducing signaling complex (DISC) (Figure 5D), whereas neither STAT3 nor STAT4 co-immunoprecipitated with Fas (Figure 5D). STAT1 also physically interacted with Fas in primary mouse CD4⁺ cells, and this was enhanced by DISC assembly (Figure 5E). Thus, STAT1, but not STAT3 or STAT4, physically interacts with Fas, and this binding is enhanced by binding of Fas to its ligand. Consistent with this observation, we also found that binding of Fas to its ligand repressed Stat1 expression early during Th cell activation (Figure S5G). Together, our findings support the idea that Fas binds and inhibits STAT1 activation and nuclear translocation (Figures 5A–C) by sequestering STAT1 at the cell membrane and thus indirectly promotes STAT3-dependent transcription required for Th17 cell differentiation.

Next, we studied the source and requirement of the FasL signal *in vitro*. At the mRNA level, *Fasl* expression showed an early peak at 1–4 hr under all differentiation conditions and was subsequently downregulated but expressed in all subsets (Figure S6A). After 96 hr of culture, Th0- and Th1-cell-differentiated cultures expressed the most *Fasl*, whereas Th17 cells

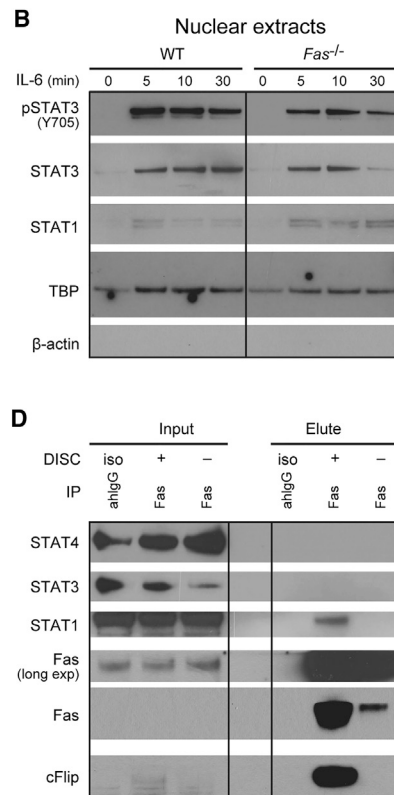


Figure 5. Fas Interacts with STAT1 and Inhibits STAT1 Phosphorylation and Nuclear Translocation

(A) Sorted naive CD4⁺CD62L^{high}CD44^{low}CD25⁻ T cells from WT and *Fas*^{-/-} mice (5×10^5 per time point) were stimulated with IL-6 as indicated. Cells were lysed and analyzed by western blotting with the indicated antibodies (Abs). Phospho-STAT1 (S727) was visualized first; the membrane was then stripped and re-probed with anti-STAT1 and anti-β-actin. One of three independent experiments is shown.

(B) Sorted naive CD4⁺ T cells (5×10^5 per time point) from WT and *Fas*^{-/-} mice were stimulated as in (A). Nuclear fractions were purified (STAR Methods) and analyzed as in (A). One of three independent experiments is shown.

(C) Sorted naive CD4⁺ T cells from WT and *Fas*^{-/-} mice were incubated with IL-6 for 30 min and stained for phospho-STAT1 (S727). Mean fluorescence of phospho-STAT1 staining per cell (left) and per nucleus (right) was quantified by confocal microscopy in >50 randomly chosen cells. One of three independent experiments is shown.

(D) EL4 cells (1×10^8 per lane) were stimulated with biotinylated hamster IgG (DISC iso) or biotinylated anti-Fas Ab (DISC⁺) and streptavidin for 15 min or left untreated on ice for 15 min (DISC⁻). Anti-Fas Ab was then added to the DISC⁻ sample. Co-immunoprecipitation (co-IP) was then performed with Protein G Magnetic Beads. Input and elute fractions from the co-IP were analyzed with the indicated Abs. One of six experiments is shown.

(E) Primary CD4⁺ T cells were MACS purified (5×10^7 per lane) and either left unstimulated on

expressed less FasL at both the mRNA (Figure S6B) and protein (Figure S6C) levels. *Fasl* expression was higher in Th1 cells than in Th17 cells, and IL-12 was unable to induce FasL expression in Th17 cells (Figures S6B and S6C). Similar to *Fas*^{-/-} cells, *Fasl*^{-/-} cells showed an increase in IFN-γ and a decrease in IL-17A production under Th1 cell and Th17 cell conditions, respectively (Figure S6D). The addition of the small-molecule compound Kp7-6, which blocks FasL with Fas interaction, also enhanced Th1 cell and reduced Th17 cell differentiation (Figure S6E). Overall, these findings suggest that the decrease in Th17 cell differentiation and increase in the Th1 cell phenotype in *Fas*^{-/-} mice depends on Fas with FasL interaction and that the ligand is present at early stages of Th cell differentiation.

Stat1 Co-deficiency Rescues the Fas-Deficiency-Mediated Effect on Th17 Cell Differentiation

To directly test the role of STAT1 in *Fas*^{-/-} T cells, we generated mice deficient in both *Stat1* and *Fas*. As previously described (Peters et al., 2015), Th17 cell differentiation was unaffected by *Stat1* deficiency (Figures 6A and 6B). The defect in IL-17A production caused by Fas deficiency was fully rescued in *Stat1*^{-/-}*Fas*^{-/-} cells under both Th17 cell differentiation conditions, although the effect was more pronounced under IL-1β, IL-6, and IL-23 conditions than under TGF-β1 and IL-6 conditions (Figures 6A and 6B). Consistent with the known role of

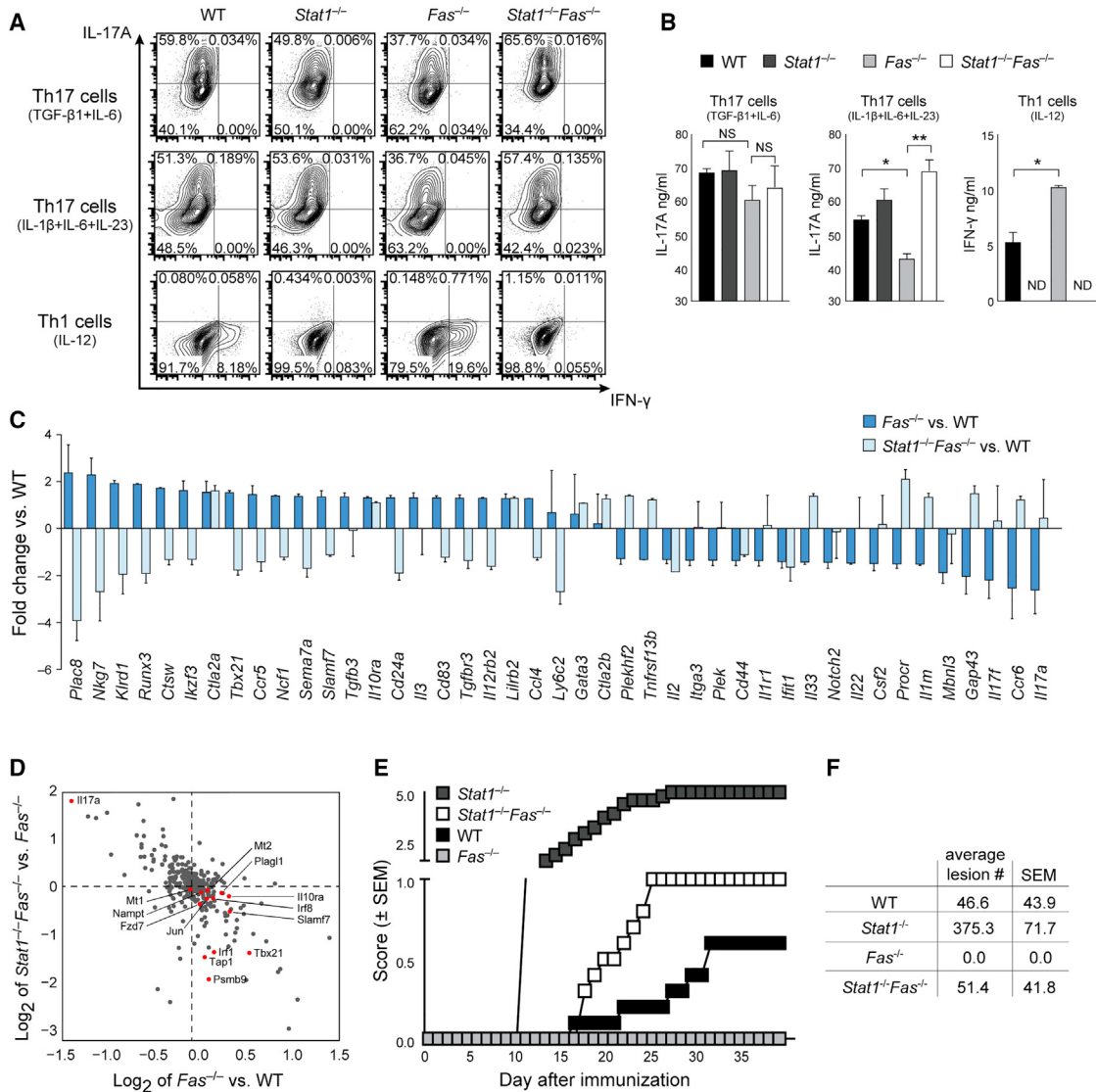


Figure 6. STAT1 Deficiency Rescues the Th17 Cell Defect of *Fas*^{-/-} CD4⁺ T Cells

(A) Naive CD4⁺CD62L^{high}CD44^{low}CD25⁻ T cells were sorted from WT, *Stat1*^{-/-}, *Fas*^{-/-}, or *Stat1*^{-/-}*Fas*^{-/-} mice, differentiated with (1) TGF-β1 and IL-6, (2) IL-1β, IL-6, and IL-23, or (3) IL-12 for 4 days, and analyzed by intracellular cytokine staining.

(B) The concentrations of IL-17A and IFN-γ in supernatants of cultures described in (A) were analyzed by ELISA.

(C) Sorted naive CD4⁺ T cells were differentiated in the presence of TGF-β1 and IL-6 for 72 hr and subjected to NanoString analysis. Transcripts with >1.25-fold regulation in *Fas*^{-/-} versus WT conditions were sorted on the basis of the *Fas*^{-/-} versus WT fold regulation (dark blue). The *Stat1*^{-/-}*Fas*^{-/-} versus WT fold regulation was then plotted for these transcripts (light blue). Data are merged from three independent experiments with one biological replicate in each experiment.

(D) The change in fold expression in NanoString in *Fas*^{-/-} versus WT samples (x axis) was plotted against *Stat1*^{-/-}*Fas*^{-/-} versus *Fas*^{-/-} samples (y axis) on a log₂ scale. Transcripts differentially expressed in the RNA-seq dataset (Figure 3) are highlighted in red. Data are merged from three independent experiments with one biological replicate in each experiment.

(E) 4×10^6 MACS-purified CD4⁺ T cells from WT, *Stat1*^{-/-}, *Fas*^{-/-}, or *Stat1*^{-/-}*Fas*^{-/-} donors were intravenously injected into *Rag1*^{-/-} mice (n = 5 per group), and 10–12 days later recipients were immunized with 100 µg MOG_{35–55} peptide. Mice were monitored daily for clinical EAE signs. One of three experiments is shown.

(F) At day 35 after immunization, inflammatory lesions in the CNS parenchyma and in the meninges were analyzed histologically. One of three experiments is shown.

Error bars indicate the mean ± SEM. *p < 0.05; **p < 0.01; ND, not detected; NS, not significant. See also Figure S6.

STAT1 in Th1 cell differentiation (Afkarian et al., 2002), IFN-γ production under Th1 cell differentiation conditions was abolished in *Stat1*^{-/-} and *Stat1*^{-/-}*Fas*^{-/-} cells (Figures 6A and 6B).

We next analyzed how *Stat1* deficiency affects the gene expression defect observed in *Fas*^{-/-} Th17 cells. Analyzing a

pre-defined 250-gene signature of Th17-cell-related transcripts (Yosef et al., 2013) showed that deficiency of both Fas and STAT1 reverted many of the expression changes induced by Fas deficiency under Th17 cell conditions. We found that the reduced expression of *Il17a* and *Il17f* and the increased

expression of *Tbx21* and *Irf1* in cells deficient in only Fas were rescued in *Stat1^{-/-}**Fas^{-/-}* cells (Figures 6C and 6D). Of note, *Ifng* overexpression was also rescued but did not reach our expression cutoff for detection in Th17 cells.

Finally, we tested the role of STAT1 in the protection from EAE in *Fas^{-/-}* mice. To specifically focus on STAT1 in CD4⁺ cells and circumvent the known susceptibility of global *Stat1^{-/-}* mice to viral infections, we reconstituted *Rag1^{-/-}* mice with purified CD4⁺ T cells deficient in Fas, Stat1, or both. Whereas mice reconstituted with *Fas^{-/-}* T cells were protected from EAE, the recipients of *Stat1^{-/-}**Fas^{-/-}* cells developed clinical signs of EAE (Figure 6E) and histologically detectable CNS lesions (Figure 6F). In line with the exacerbated development of EAE in *Stat1^{-/-}* mice (Bettelli et al., 2004), recipients of *Stat1^{-/-}* cells developed severe EAE (Figure 6E) and a high number of histological lesions (Figure 6F) and had to be sacrificed early. The defect in Th17 cell differentiation in *Fas^{-/-}* T cells thus dominantly depends on the excessive presence of STAT1 and can be rescued by *Stat1* deletion *in vivo*. This identifies a mechanistic model whereby Fas controls the Th17-to-Th1 cell balance and autoimmunity through STAT1.

DISCUSSION

In this study, we demonstrated that Fas deficiency impaired Th17 cell differentiation and grossly attenuated EAE while enhancing Th1 cell generation. This effect appeared to be apoptosis independent. Computational modeling identified a Th1-cell-like gene expression signature in *Fas^{-/-}* Th17 cells and nominated STAT1 as a top inferred transcriptional regulator of this signature. Indeed, we showed that Fas physically interacted with STAT1 and that loss of Fas increased STAT1 activation, whereas deficiency of both STAT1 and Fas rescued the Th17 defect. Consistent with these *in vitro* data, EAE susceptibility was restored in mice replete with CD4⁺ T cells deficient in both Fas and STAT1. Our findings thus emphasize an apoptosis-independent function of Fas whereby Fas regulates the balance between antagonizing STAT1 and STAT3 and competing differentiation programs in different Th subsets and consequently organ-specific autoimmunity.

The link we established here between Fas and STAT1 signaling provides a mechanistic explanation for the long-standing conundrum that *Fas^{-/-}* mice are almost completely protected from EAE (Waldner et al., 1997). The excessive STAT1 activation in *Fas^{-/-}* cells impairs the differentiation and stability of Th17 cells, which are an essential driver of EAE (Cua et al., 2003; Lee et al., 2012). Our observations suggest a dual effect of Fas on STAT1: First, naive *Fas^{-/-}* cells express more STAT1, indicating that Fas continuously represses STAT1 activation and self-induction in naive T cells. Second, cytokines (e.g., IL-6) further enhance STAT1 activation, and this is dis-inhibited in the absence of Fas. Thus, loss of Fas results in overwhelming STAT1 activation even under Th17 cell differentiation conditions, resulting in the repression of pro-inflammatory Th17 cells.

The function of IFN- γ -producing T cells in the CNS during EAE is complex and partly unresolved (Korn and Kallies, 2017). Mice deficient in IFN- γ , IFN- γ receptor, and STAT1 all develop more severe EAE (Bettelli et al., 2004; Tran et al., 2000), which was

one of the observations that initially sparked the discovery of Th17 cells and argues for a protective role of Th1 cells in EAE. In contrast, the occurrence of cells that produce both IL-17A and IFN- γ in the CNS correlates with disease severity in EAE, and these cells are mostly derived from cells that produce only IL-17A (Hirota et al., 2011). Induction of IFN- γ in Th17 cells is thought to be induced by activation of STAT4 by IL-23 in Th17 cells. IL-17A⁺IFN- γ ⁺ cells are thought to be pathogenic, although deletion of T-bet reduces their occurrence without considerably affecting EAE severity (Brucklacher-Waldert et al., 2016; Duhen et al., 2013). On the basis of our fate-reporting experiments, global Fas deficiency induces IFN- γ ⁺ cells before they can reach the Th17 lineage, whereas Th17-restricted Fas deficiency causes Th17-to-Th1 instability. Both of these processes appear to inhibit the development of EAE. Of note, Fas deficiency induces a greater extent of protection from EAE than deficiency of IL-17A or IL-17F (Haak et al., 2009; Komiyama et al., 2006). Indeed, we previously identified a molecular signature that distinguishes pathogenic from non-pathogenic Th17 cells (Gaublomme et al., 2015; Lee et al., 2012). Preferential activation of STAT1 in *Fas^{-/-}* mice not only induces T-bet and a Th1-cell-like phenotype but also interferes with the STAT3-mediated Th17 cell differentiation program, thereby altering the phenotype and reducing the pathogenicity of Th17 cells *in vivo*.

Th17 cell development is critically dependent on STAT3 (Harris et al., 2007; Mathur et al., 2007), and humans with dominant-negative mutations of STAT3 develop hyper-immunoglobulin E syndrome, characterized by impaired Th17 differentiation and greater susceptibility to fungal infections (Ma et al., 2008; Milner et al., 2008). STAT1 and STAT3 heterodimerize, and increased STAT1 signaling inhibit STAT3-dependent transcription-driving Th17 cells (Villarino et al., 2017). Two recent studies demonstrated that STAT1 not only cross-inhibits STAT3-dependent transcription but also dictates the specificity of the cytokines signaling through both STAT1 and STAT3 (Hirahara et al., 2015; Peters et al., 2015). Indeed, patients with STAT1 gain-of-function mutations show impaired Th17 cell responses and develop chronic fungal infections (Liu et al., 2011). Thus, STAT3 loss of function and STAT1 gain of function both impair Th17 cell responses. We found here that Fas was critical for sequestering STAT1, therefore tipping the balance in favor of STAT3's promotion of the Th17 cell differentiation program. However, loss of Fas released STAT1, and we predict that this excessive availability of STAT1 in turn inhibits the Th17 cell gene program and promotes Th1 cell differentiation. Our data also suggest that Fas controls the differentiation of other Th cell lineages and could thus be a regulator of multiple Th cell lineages through cross-inhibition of STAT proteins.

We found Fas expression to be induced by activation alone and to be additionally regulated by cytokines. We identified TGF- β 1 to actively represses Fas expression, which could explain why iTreg cell differentiation is unaffected by Fas deficiency and why Th17 cells generated with TGF- β 1 and IL-6 are less affected than Th17 cells differentiated with IL-1 β , IL-6, and IL-23. Consequently, Th1 cells are equipped with a greater density of ligand and receptor molecules than Th17 cells. However, cells co-expressing FasL and Fas do not die when sufficient survival signals are present, and Fas receptor binding can have pro-proliferative effects under suboptimal TCR stimulation

conditions (Kennedy et al., 1999; Paulsen et al., 2011). It could be under such conditions that Fas expression in Th cells limits commitment to the Th1 cell differentiation pathway by inhibiting STAT1 activation.

Several observations argue against a link between the defect of Th17 cell differentiation and lupus-like systemic autoimmunity in *Fas*^{-/-} mice. First, *Fas*^{-/-} mice were protected from EAE already at 6–10 weeks of age, which is before autoimmunity manifests on this genetic background (Cohen and Eisenberg, 1991). Second, T-cell-specific Fas deficiency in *Cd4*^{cre}*Fas*^{f/f} mice was sufficient to impair Th17 cell responses without triggering autoimmunity (Hao et al., 2004). Third, limiting Fas deficiency to Th17 cells by utilizing an *Il17a*^{cre} mouse line affected their function in a cell-intrinsic manner but did not induce autoimmunity (data not shown). We have thus demonstrated here that the ability of Fas to suppress lupus-like autoimmunity can be segregated from its Th17-cell-promoting function.

Reciprocal and antagonizing development is an essential and common theme in the directed differentiation of Th cell lineages (Bettelli et al., 2006b; O’Shea and Paul, 2010). Our previous transcriptional model predicted that positive regulators of Th17 cell differentiation would negatively affect other Th cell lineages and vice versa (Yosef et al., 2013). How can this be achieved? On a cell-extrinsic level, cytokines produced by one subset can cross-regulate differentiation of the other, and evidence for this cell-extrinsic cross-regulation has been overwhelming (e.g., Zhu et al., 2010). However, in this report, we have provided evidence of how this is achieved in a cell-intrinsic manner: Fas was induced during Th17 cell differentiation, sequestered STAT1, and thereby limited Th1 cell differentiation and indirectly promoted Th17 differentiation.

In conclusion, we have identified Fas as a cell-intrinsic switch that not only regulates apoptosis but also regulates competing differentiation pathways of Th cell subsets in a cell-intrinsic manner. Our study also provides a link between Fas and STAT1 signaling and a mechanistic explanation of why *Fas*^{-/-} mice are resistant to EAE yet are susceptible to systemic autoimmunity.

STAR METHODS

Detailed methods are provided in the online version of this paper and include the following:

- KEY RESOURCES TABLE
- CONTACT FOR REAGENT AND RESOURCE SHARING
- EXPERIMENTAL MODEL AND SUBJECT DETAILS
 - Experimental Animals
 - Experimental Autoimmune Encephalomyelitis
- METHOD DETAILS
 - Isolation of CNS-Infiltrating Mononuclear Cells
 - CNS Histology
 - Enzyme-Linked Immunosorbent Assay
 - Flow Cytometry and Related Reagents
 - Isolation and Differentiation of Naive CD4⁺ T Cells
 - Immunofluorescence Microscopy
 - Constructs and Luciferase Assays
 - RNA Quantification Using nCounter and qPCR Analysis

- RNA Sequencing
- Transcriptional and Gene Set Enrichment Analysis
- Inferred Transcriptional Regulators
- Protein-Protein Interaction Data and Network Reconstruction
- Co-immunoprecipitation and Western Blotting
- QUANTIFICATION AND STATISTICAL ANALYSIS
 - Statistics
- DATA AND SOFTWARE AVAILABILITY

SUPPLEMENTAL INFORMATION

Supplemental Information includes six figures and one table and can be found with this article online at <https://doi.org/10.1016/j.immuni.2018.03.008>.

ACKNOWLEDGMENTS

We thank Deneen Kozoriz for cell sorting. We thank Dr. Jin Wang (Department of Pharmacology, Baylor College of Medicine) for providing us with the *Fas*^{fl/fl} mouse line. We thank Leslie Gaffney (Broad Institute of MIT and Harvard) for helping with figure editing. G.M.z.H. was funded in part by the Deutsche Forschungsgemeinschaft (DFG; grant ME4050/1-1) and a National Multiple Sclerosis Society postdoctoral fellowship (grant FG20118-A-1). M.A.S. was funded in part by DFG grant SCHR 1481/1-1. Work was supported by the Klarman Cell Observatory at the Broad Institute (to A.R. and V.K.K.) and the Howard Hughes Medical Institute (to A.R.). V.K.K. received funding from NIH grants RO1 NS30843, P01 AI0562999, P01 NS076410, P01 AI039671, P01 AI045757, and P01 AI073748.

AUTHOR CONTRIBUTIONS

G.M.z.H., M.A.S., A.S., C.W., Y.L., and R.S. performed experiments. D.P. and A.R. performed computational analysis. G.M.z.H., A.R., and V.K.K. conceived the study. G.M.z.H., A.R., and V.K.K. wrote the manuscript.

DECLARATION OF INTERESTS

A.R. is a member of the scientific advisory board for ThermoFisher Scientific, Driver Group, and Syros Pharmaceuticals.

Received: December 1, 2017

Revised: February 28, 2018

Accepted: March 2, 2018

Published: March 20, 2018

REFERENCES

- Afkarian, M., Sedy, J.R., Yang, J., Jacobson, N.G., Cereb, N., Yang, S.Y., Murphy, T.L., and Murphy, K.M. (2002). T-bet is a STAT1-induced regulator of IL-12R expression in naïve CD4⁺ T cells. *Nat. Immunol.* 3, 549–557.
- Benjamini, Y., and Yekutieli, D. (2001). The control of the false discovery rate in multiple testing under dependency. *Ann. Stat.* 29, 1165–1188.
- Bettelli, E., Pagany, M., Weiner, H.L., Linington, C., Sobel, R.A., and Kuchroo, V.K. (2003). Myelin oligodendrocyte glycoprotein-specific T cell receptor transgenic mice develop spontaneous autoimmune optic neuritis. *J. Exp. Med.* 197, 1073–1081.
- Bettelli, E., Sullivan, B., Szabo, S.J., Sobel, R.A., Glimcher, L.H., and Kuchroo, V.K. (2004). Loss of T-bet, but not STAT1, prevents the development of experimental autoimmune encephalomyelitis. *J. Exp. Med.* 200, 79–87.
- Bettelli, E., Baeten, D., Jäger, A., Sobel, R.A., and Kuchroo, V.K. (2006a). Myelin oligodendrocyte glycoprotein-specific T and B cells cooperate to induce a Devic-like disease in mice. *J. Clin. Invest.* 116, 2393–2402.
- Bettelli, E., Carrier, Y., Gao, W., Korn, T., Strom, T.B., Oukka, M., Weiner, H.L., and Kuchroo, V.K. (2006b). Reciprocal developmental pathways for the generation of pathogenic effector TH17 and regulatory T cells. *Nature* 441, 235–238.

- Brucklacher-Waldert, V., Ferreira, C., Innocentini, S., Kamdar, S., Withers, D.R., Kullberg, M.C., and Veldhoen, M. (2016). Tbet or Continued ROR γ T Expression Is Not Required for Th17-Associated Immunopathology. *J. Immunol.* 196, 4893–4904.
- Cencioni, M.T., Santini, S., Ruocco, G., Borsellino, G., De Bardi, M., Grasso, M.G., Ruggieri, S., Gasperini, C., Centonze, D., Barilà, D., et al. (2015). FAS-ligand regulates differential activation-induced cell death of human T-helper 1 and 17 cells in healthy donors and multiple sclerosis patients. *Cell Death Dis.* 6, e1741.
- Cohen, P.L., and Eisenberg, R.A. (1991). Lpr and gld: single gene models of systemic autoimmunity and lymphoproliferative disease. *Annu. Rev. Immunol.* 9, 243–269.
- Cua, D.J., Sherlock, J., Chen, Y., Murphy, C.A., Joyce, B., Seymour, B., Lucian, L., To, W., Kwan, S., Churakova, T., et al. (2003). Interleukin-23 rather than interleukin-12 is the critical cytokine for autoimmune inflammation of the brain. *Nature* 421, 744–748.
- Duhen, R., Glatigny, S., Arbelaez, C.A., Blair, T.C., Oukka, M., and Bettelli, E. (2013). Cutting edge: the pathogenicity of IFN- γ -producing Th17 cells is independent of T-bet. *J. Immunol.* 190, 4478–4482.
- Eppig, J.T., Blake, J.A., Bult, C.J., Kadin, J.A., and Richardson, J.E.; Mouse Genome Database Group (2015). The Mouse Genome Database (MGD): facilitating mouse as a model for human biology and disease. *Nucleic Acids Res.* 43, D726–D736.
- Fortner, K.A., and Budd, R.C. (2005). The death receptor Fas (CD95/APO-1) mediates the deletion of T lymphocytes undergoing homeostatic proliferation. *J. Immunol.* 175, 4374–4382.
- Gaublomme, J.T., Yosef, N., Lee, Y., Gerther, R.S., Yang, L.V., Wu, C., Pandolfi, P.P., Mak, T., Satija, R., Shalek, A.K., et al. (2015). Single-Cell Genomics Unveils Critical Regulators of Th17 Cell Pathogenicity. *Cell* 163, 1400–1412.
- Ghoreschi, K., Laurence, A., Yang, X.P., Tato, C.M., McGeechey, M.J., Konkel, J.E., Ramos, H.L., Wei, L., Davidson, T.S., Bouladoux, N., et al. (2010). Generation of pathogenic T(H)17 cells in the absence of TGF- β signalling. *Nature* 467, 967–971.
- Haak, S., Croxford, A.L., Kreymborg, K., Heppner, F.L., Pouly, S., Becher, B., and Waisman, A. (2009). IL-17A and IL-17F do not contribute vitally to autoimmune neuro-inflammation in mice. *J. Clin. Invest.* 119, 61–69.
- Hao, Z., Hampel, B., Yagita, H., and Rajewsky, K. (2004). T cell-specific ablation of Fas leads to Fas ligand-mediated lymphocyte depletion and inflammatory pulmonary fibrosis. *J. Exp. Med.* 199, 1355–1365.
- Harris, T.J., Grosso, J.F., Yen, H.R., Xin, H., Kortylewski, M., Albesiano, E., Hippkiss, E.L., Getnet, D., Goldberg, M.V., Maris, C.H., et al. (2007). Cutting edge: An in vivo requirement for STAT3 signaling in TH17 development and TH17-dependent autoimmunity. *J. Immunol.* 179, 4313–4317.
- Hirahara, K., Onodera, A., Villarino, A.V., Bonelli, M., Sciumè, G., Laurence, A., Sun, H.W., Brooks, S.R., Vahedi, G., Shih, H.Y., et al. (2015). Asymmetric Action of STAT Transcription Factors Drives Transcriptional Outputs and Cytokine Specificity. *Immunity* 42, 877–889.
- Hirota, K., Duarte, J.H., Veldhoen, M., Hornsby, E., Li, Y., Cua, D.J., Ahlfors, H., Wilhelm, C., Tolaini, M., Menzel, U., et al. (2011). Fate mapping of IL-17-producing T cells in inflammatory responses. *Nat. Immunol.* 12, 255–263.
- Holzelova, E., Vonarbourg, C., Stolzenberg, M.C., Arkwright, P.D., Selz, F., Prieur, A.M., Blanche, S., Bartunkova, J., Vilmer, E., Fischer, A., et al. (2004). Autoimmune lymphoproliferative syndrome with somatic Fas mutations. *N. Engl. J. Med.* 351, 1409–1418.
- Hu, X., and Ivashkov, L.B. (2009). Cross-regulation of signaling pathways by interferon-gamma: implications for immune responses and autoimmune diseases. *Immunity* 31, 539–550.
- Jäger, A., Dardalhon, V., Sobel, R.A., Bettelli, E., and Kuchroo, V.K. (2009). Th1, Th17, and Th9 effector cells induce experimental autoimmune encephalomyelitis with different pathological phenotypes. *J. Immunol.* 183, 7169–7177.
- Kano, S., Sato, K., Morishita, Y., Vollstedt, S., Kim, S., Bishop, K., Honda, K., Kubo, M., and Taniguchi, T. (2008). The contribution of transcription factor IRF1 to the interferon-gamma-interleukin 12 signaling axis and TH1 versus TH-17 differentiation of CD4+ T cells. *Nat. Immunol.* 9, 34–41.
- Kennedy, N.J., Kataoka, T., Tschoopp, J., and Budd, R.C. (1999). Caspase activation is required for T cell proliferation. *J. Exp. Med.* 190, 1891–1896.
- Komiyama, Y., Nakae, S., Matsuki, T., Nambu, A., Ishigame, H., Kakuta, S., Sudo, K., and Iwakura, Y. (2006). IL-17 plays an important role in the development of experimental autoimmune encephalomyelitis. *J. Immunol.* 177, 566–573.
- Korn, T., and Kallies, A. (2017). T cell responses in the central nervous system. *Nat. Rev. Immunol.* 17, 179–194.
- Korn, T., Bettelli, E., Oukka, M., and Kuchroo, V.K. (2009). IL-17 and Th17 Cells. *Annu. Rev. Immunol.* 27, 485–517.
- Langmead, B., and Salzberg, S.L. (2012). Fast gapped-read alignment with Bowtie 2. *Nat. Methods* 9, 357–359.
- Lee, Y., Awasthi, A., Yosef, N., Quintana, F.J., Xiao, S., Peters, A., Wu, C., Kleinewietfeld, M., Kunder, S., Hafler, D.A., et al. (2012). Induction and molecular signature of pathogenic TH17 cells. *Nat. Immunol.* 13, 991–999.
- Lee, Y., Mitsdoerffer, M., Xiao, S., Gu, G., Sobel, R.A., and Kuchroo, V.K. (2015). IL-21R signaling is critical for induction of spontaneous experimental autoimmune encephalomyelitis. *J. Clin. Invest.* 125, 4011–4020.
- Levin, J.Z., Yassour, M., Adiconis, X., Nusbaum, C., Thompson, D.A., Friedman, N., Gnrke, A., and Regev, A. (2010). Comprehensive comparative analysis of strand-specific RNA sequencing methods. *Nat. Methods* 7, 709–715.
- Liu, L., Okada, S., Kong, X.F., Kreins, A.Y., Cypowyj, S., Abhyankar, A., Toubiana, J., Itan, Y., Audry, M., Nitschke, P., et al. (2011). Gain-of-function human STAT1 mutations impair IL-17 immunity and underlie chronic mucocutaneous candidiasis. *J. Exp. Med.* 208, 1635–1648.
- Ma, C.S., Chew, G.Y., Simpson, N., Priyadarshi, A., Wong, M., Grimbacher, B., Fulcher, D.A., Tangye, S.G., and Cook, M.C. (2008). Deficiency of Th17 cells in hyper IgE syndrome due to mutations in STAT3. *J. Exp. Med.* 205, 1551–1557.
- Maslov, S., and Sneppen, K. (2002). Specificity and stability in topology of protein networks. *Science* 296, 910–913.
- Mathur, A.N., Chang, H.C., Zisoulis, D.G., Stritesky, G.L., Yu, Q., O'Malley, J.T., Kapur, R., Levy, D.E., Kansas, G.S., and Kaplan, M.H. (2007). Stat3 and Stat4 direct development of IL-17-secreting Th cells. *J. Immunol.* 178, 4901–4907.
- Matys, V., Kel-Margoulis, O.V., Fricke, E., Liebich, I., Land, S., Barre-Dirrie, A., Reuter, I., Chekmenev, D., Krull, M., Hornischer, K., et al. (2006). TRANSFAC and its module TRANSCompel: transcriptional gene regulation in eukaryotes. *Nucleic Acids Res.* 34, D108–D110.
- Meyer Zu Horste, G., Wu, C., Wang, C., Cong, L., Pawlak, M., Lee, Y., Elyaman, W., Xiao, S., Regev, A., and Kuchroo, V.K. (2016). RBPJ Controls Development of Pathogenic Th17 Cells by Regulating IL-23 Receptor Expression. *Cell Rep.* 16, 392–404.
- Milner, J.D., Brenchley, J.M., Laurence, A., Freeman, A.F., Hill, B.J., Elias, K.M., Kanno, Y., Spalding, C., Elloumi, H.Z., Paulson, M.L., et al. (2008). Impaired T(H)17 cell differentiation in subjects with autosomal dominant hyper-IgE syndrome. *Nature* 452, 773–776.
- O'Shea, J.J., and Paul, W.E. (2010). Mechanisms underlying lineage commitment and plasticity of helper CD4+ T cells. *Science* 327, 1098–1102.
- Paulsen, M., Valentín, S., Mathew, B., Adam-Klages, S., Bertsch, U., Lavrik, I., Krammer, P.H., Kabelitz, D., and Janssen, O. (2011). Modulation of CD4+ T-cell activation by CD95 co-stimulation. *Cell Death Differ.* 18, 619–631.
- Peters, A., Fowler, K.D., Chalmin, F., Merkler, D., Kuchroo, V.K., and Pot, C. (2015). IL-27 Induces Th17 Differentiation in the Absence of STAT1 Signaling. *J. Immunol.* 195, 4144–4153.
- Sabelko, K.A., Kelly, K.A., Nahm, M.H., Cross, A.H., and Russell, J.H. (1997). Fas and Fas ligand enhance the pathogenesis of experimental allergic encephalomyelitis, but are not essential for immune privilege in the central nervous system. *J. Immunol.* 159, 3096–3099.
- Strasser, A., Jost, P.J., and Nagata, S. (2009). The many roles of FAS receptor signaling in the immune system. *Immunity* 30, 180–192.

- Subramanian, A., Tamayo, P., Mootha, V.K., Mukherjee, S., Ebert, B.L., Gillette, M.A., Paulovich, A., Pomeroy, S.L., Golub, T.R., Lander, E.S., and Mesirov, J.P. (2005). Gene set enrichment analysis: a knowledge-based approach for interpreting genome-wide expression profiles. *Proc. Natl. Acad. Sci. USA* **102**, 15545–15550.
- Takahashi, T., Tanaka, M., Brannan, C.I., Jenkins, N.A., Copeland, N.G., Suda, T., and Nagata, S. (1994). Generalized lymphoproliferative disease in mice, caused by a point mutation in the Fas ligand. *Cell* **76**, 969–976.
- Tran, E.H., Prince, E.N., and Owens, T. (2000). IFN-gamma shapes immune invasion of the central nervous system via regulation of chemokines. *J. Immunol.* **164**, 2759–2768.
- Trapnell, C., Pachter, L., and Salzberg, S.L. (2009). TopHat: discovering splice junctions with RNA-Seq. *Bioinformatics* **25**, 1105–1111.
- Trapnell, C., Williams, B.A., Pertea, G., Mortazavi, A., Kwan, G., van Baren, M.J., Salzberg, S.L., Wold, B.J., and Pachter, L. (2010). Transcript assembly and quantification by RNA-Seq reveals unannotated transcripts and isoform switching during cell differentiation. *Nat. Biotechnol.* **28**, 511–515.
- Villarino, A.V., Kanno, Y., and O’Shea, J.J. (2017). Mechanisms and consequences of Jak-STAT signaling in the immune system. *Nat. Immunol.* **18**, 374–384.
- Waldner, H., Sobel, R.A., Howard, E., and Kuchroo, V.K. (1997). Fas- and FasL-deficient mice are resistant to induction of autoimmune encephalomyelitis. *J. Immunol.* **159**, 3100–3103.
- Waldner, H., Collins, M., and Kuchroo, V.K. (2004). Activation of antigen-presenting cells by microbial products breaks self tolerance and induces autoimmune disease. *J. Clin. Invest.* **113**, 990–997.
- Walsh, C.M., Wen, B.G., Chinnaiyan, A.M., O’Rourke, K., Dixit, V.M., and Hedrick, S.M. (1998). A role for FADD in T cell activation and development. *Immunity* **8**, 439–449.
- Wang, Y., Wu, T.R., Cai, S., Welte, T., and Chin, Y.E. (2000). Stat1 as a component of tumor necrosis factor alpha receptor 1-TRADD signaling complex to inhibit NF- κ B activation. *Mol. Cell. Biol.* **20**, 4505–4512.
- Watanabe-Fukunaga, R., Brannan, C.I., Copeland, N.G., Jenkins, N.A., and Nagata, S. (1992). Lymphoproliferation disorder in mice explained by defects in Fas antigen that mediates apoptosis. *Nature* **356**, 314–317.
- Xiao, S., Yosef, N., Yang, J., Wang, Y., Zhou, L., Zhu, C., Wu, C., Baloglu, E., Schmidt, D., Ramesh, R., et al. (2014). Small-molecule ROR γ t antagonists inhibit T helper 17 cell transcriptional network by divergent mechanisms. *Immunity* **40**, 477–489.
- Yang, X.O., Panopoulos, A.D., Nurieva, R., Chang, S.H., Wang, D., Watowich, S.S., and Dong, C. (2007). STAT3 regulates cytokine-mediated generation of inflammatory helper T cells. *J. Biol. Chem.* **282**, 9358–9363.
- Yosef, N., Shalek, A.K., Gaublomme, J.T., Jin, H., Lee, Y., Awasthi, A., Wu, C., Karwacz, K., Xiao, S., Jorgolli, M., et al. (2013). Dynamic regulatory network controlling TH17 cell differentiation. *Nature* **496**, 461–468.
- Zhang, F., Meng, G., and Strober, W. (2008). Interactions among the transcription factors Runx1, RORgammat and Foxp3 regulate the differentiation of interleukin 17-producing T cells. *Nat. Immunol.* **9**, 1297–1306.
- Zheng, Y., Ouaz, F., Bruzzo, P., Singh, V., Gerondakis, S., and Beg, A.A. (2001). NF- κ B RelA (p65) is essential for TNF-alpha-induced fas expression but dispensable for both TCR-induced expression and activation-induced cell death. *J. Immunol.* **166**, 4949–4957.
- Zhu, J., Yamane, H., and Paul, W.E. (2010). Differentiation of effector CD4 T cell populations (*). *Annu. Rev. Immunol.* **28**, 445–489.

STAR★METHODS

KEY RESOURCES TABLE

REAGENT or RESOURCE	SOURCE	IDENTIFIER
Antibodies		
Rat monoclonal anti-IL-17A (clone TC11-18H10.1)	BioLegend	Cat#506916; RRID: AB_536018
Rat monoclonal anti-IFN- γ (clone XMG1.2)	BioLegend	Cat#505813; RRID: AB_493312
Mouse monoclonal anti-pSTAT3 Y705 (clone 4/P-STAT3)	BD	Cat#612569; RRID: AB_399860
Rat monoclonal anti-Foxp3 (clone FJK-16s)	eBioscience	Cat#12-5773-82; RRID: AB_465936
Hamster monoclonal anti-Fas (clone Jo2, biotinylated)	BioLegend	Cat#554257
Rat monoclonal anti-V α 3.2 (clone RR3-16)	BioLegend	Cat#135404; RRID: AB_1937235
Rat monoclonal anti-V β 11 (clone RR3-15)	BD	Cat#553198; RRID: AB_394704
Rat monoclonal anti-IL-13 (clone eBio13A)	eBioscience	Cat#12-7133-82; RRID: AB_763559
Rabbit polyclonal anti-STAT1	CST	Cat#9172; RRID: AB_10693929
rabbit monoclonal anti-S727-phospho-STAT1 (clone D3B7)	CST	Cat#8826
rabbit monoclonal anti-Y701-phospho-STAT1 (clone 58D6)	CST	Cat#9167; RRID: AB_561284
rabbit monoclonal anti-Y705-phospho-STAT3 (clone D3A7)	CST	Cat# 9145; RRID: AB_2491009
rabbit monoclonal anti-STAT3 (clone D3Z2G)	CST	Cat#12640; RRID: AB_2629499
rabbit monoclonal anti-STAT4 (clone C46B10)	CST	Cat#2653; RRID: AB_2255156
rat monoclonal anti-Fas (clone 7C10)	EMD Millipore	Cat#05-351
Chemicals, Peptides, and Recombinant Proteins		
myelin oligodendrocyte glycoprotein peptide MOG _{35–55}	Quality Controlled Biochemicals	N/A
Adjuvant, Complete (Freund)	BD Difco	Cat#263810
<i>M. tuberculosis</i> H37Ra extract	BD Difco	Cat#231141
Pertussis toxin	List Biological Laboratories	Cat#180
Caspase 1 inhibitor (Z-YVAD-FMK)	EMD Millipore	Cat# 218746
Caspase 3 inhibitor (Z-DEVD-FMK)	EMD Millipore	Cat# 264155; CAS 210344-95-9
Caspase 8 inhibitor (Z-IETD-FMK)	EMD Millipore	Cat# 218759; CAS 210344-98-2
Fas/FasL antagonist (Kp7-6)	EMD Millipore	Cat#341291
MegaFasL	Adipogen	Cat#AG-40B-0130-C010
Critical Commercial Assays		
Dual-Luciferase Reporter Assay System	Promega	Cat#E1910
Nanostring nCounter	NanoString Technologies	N/A
Deposited Data		
Raw RNA-sequencing data	This paper	GEO: GSE111244
Experimental Models: Cell Lines		
Mouse: EL4 cells	ATCC	TIB-39
Experimental Models: Organisms/Strains		
Mouse: Cd4 ^{cre} ; B6.Cg-Tg(Cd4-cre)1Cwi/Bflu	Taconic	Cat#017336
Mouse: CD45.1: B6.SJL-Ptprc ^a Pepc ^b /BoyJ	Jackson	Cat#002014
Mouse: CD90.1: B6.PL-Thy1 ^a /CyJ	Jackson	Cat#000406
Mouse: Fas ^{-/-} : B6.MRL-Tnfrsf6 ^{lpr} /J	Jackson	Cat#000482
Mouse: Fasl ^{-/-} : B6Smm.C3-Fasl ^{gld} /J	Jackson	Cat#001021
Mouse: Rag1 ^{-/-} : B6.129S7-Rag1 ^{tm1Mm0} /J	Jackson	Cat#002216
Mouse: R26 ^{RFP} : B6.129S6-Gt(ROSA)26Sor ^{tm1(CAG-tdTomato)Hze} /J	Jackson	Cat#007905
Mouse: Stat1 ^{-/-} : B6.129S(Cg)-Stat1 ^{tm1Dlv} /J	Jackson	Cat#012606
Mouse: Fas ^{flx} : C57BL/6-Fas ^{tm1Cgn}	Baylor College	
Mouse: II17a ^{cre} ; II17a ^{tm1.1(icre)Stck} /J	Jackson	Cat#016879

(Continued on next page)

Continued

REAGENT or RESOURCE	SOURCE	IDENTIFIER
Mouse: 2D2: C57BL/6-Tg(Tcra2D2,Tcrb2D2)1Kuch	Generated in the lab	Cat#006912
Mouse: Casp3 ^{-/-} : B6N.129S1-Casp3 ^{tm1Flv} /J	Jackson	Cat#006233
Oligonucleotides		
TaqMan primer/probe <i>Stat1</i>	BD	Cat#Mm01257286_m1
TaqMan primer/probe <i>Fasl</i>	BD	Cat#Mm00438864_m1
TaqMan primer/probe <i>Fas</i>	BD	Cat#Mm01204974_m1
Recombinant DNA		
Plasmid: pCMV-Stat1	PlasmID Repository	MmCD00312753
Plasmid: pCMV-Stat3	PlasmID Repository	MmCD00312996
Plasmid pGL4-II17a	(Zhang et al., 2008)	Addgene Plasmid #20124
Software and Algorithms		
TopHat (version 2.0.10)	(Trapnell et al., 2009)	https://ccb.jhu.edu/software/tophat/index.shtml
Bowtie (version 2.1.0.0)	(Langmead and Salzberg, 2012)	http://bowtie-bio.sourceforge.net/bowtie2/index.shtml
Cuffdiff (version 2.1.1)	(Trapnell et al., 2010)	http://cole-trapnell-lab.github.io/cufflinks/cuffdiff/

CONTACT FOR REAGENT AND RESOURCE SHARING

Further information and requests for resources and reagents should be directed to and will be fulfilled by the Lead Contact, Dr. Vijay K. Kuchroo (vkuchroo@evergrande.hms.harvard.edu).

EXPERIMENTAL MODEL AND SUBJECT DETAILS**Experimental Animals**

B6.Cg-Tg(Cd4-cre)1Cwi/BfluJ (named *Cd4*^{cre}) mice were purchased from Taconic. C57BL/6J, B6.SJL-Ptprc^aPepc^b/BoyJ (named CD45.1), B6.PL-Thy1^a/CyJ (named CD90.1), B6.MRL-Tnfrsf6^{lpr}/J (i.e., *lpr* mice on the C57BL/6 background; named *Fas*^{-/-} in the manuscript), B6Smn.C3-Fas^{gld}/J (i.e., *gld* mice on the C57BL/6 background; named *Fasl*^{-/-}), B6N.129S1-Casp3^{tm1Flv}/J (named Casp3^{-/-}), B6.129S7-Rag1^{tm1Mom}/J (named *Rag1*^{-/-}), B6;129S6-Gt(ROSA)26Sor^{tm9(CAG-tdTomato)Hze}/J (named *R26*^{RFP}), B6.129S(Cg)-Stat1^{tm1Dlv}/J (named *Stat1*^{-/-}) mice, and *Il17a*^{tm1.1(cre)Stck}/J (named *Il17a*^{cre}) were purchased from The Jackson Laboratories. C57BL/6-*Fas*^{tm1Cgn}/J mice (named *Fas*^{f/f}) were described before (Hao et al., 2004) and were provided by Dr. Jin Wang, Baylor College of Medicine. C57BL/6-Tg(Tcra2D2,Tcrb2D2)1Kuch/J (named 2D2) mice have been previously described (Bettelli et al., 2006a). *Fas*^{-/-} mice were crossed with 2D2 mice to generate *Fas*^{-/-}2D2 mice and with *Stat1*^{-/-} mice to generate *Fas*^{-/-}*Stat1*^{-/-} mice. CD45.1 mice were crossed with 2D2 mice to generate CD45.1-2D2 mice. C57BL/6J mice were used as wildtype controls for *Fas*^{-/-} and *Casp3*^{-/-} mice. For repletion experiments, 4×10^6 MACS purified CD4⁺ T cells were intravenously injected into *Rag1*^{-/-} mice. 10–12 days after repletion, peripheral blood was analyzed for the presence of CD3⁺CD4⁺ cells and EAE was actively induced (see below). Cre negative *Fas*^{f/f} littermates were used as controls for *Cd4*^{cre}*Fas*^{f/f} mice. Littermates heterozygous for both the *Il17a*^{cre} allele and for the *Fas*^{fl/fl} allele were used as controls for the *Il17a*^{cre}*Fas*^{f/f} mice. Genotyping was done by routine PCR from tail biopsy derived DNA. All experiments were approved by and carried out in accordance with guidelines of the Institutional Animal Care and Use Committee (IACUC) at Harvard Medical School.

Experimental Autoimmune Encephalomyelitis

Mice (6–10 weeks old) of both sexes at balanced ratio were immunized s.c. in the flanks with an emulsion containing the myelin oligodendrocyte glycoprotein (MOG) peptide MOG_{35–55} (100 µg/mouse, Quality Controlled Biochemicals, >80% purity) and *M. tuberculosis* H37Ra extract (5 mg/mL, Difco Laboratories) in CFA (200 µL/mouse). Pertussis toxin (200 ng/mouse, List Biological Laboratories) was administered i.p. on days 0 and 2. Adoptive transfer EAE of Th17 cell differentiated 2D2 cells was performed as described (Jäger et al., 2009). Briefly, CD4⁺CD44^{low}CD62L^{high}CD25⁻ naive CD4⁺ T cells were purified by FACS sorting from 2D2 donor mice and cultured at 2×10^6 / mL in the presence of irradiated antigen presenting cells, soluble anti-CD3 antibody (2.5 µg/mL), IL-6 (30 ng/mL), TGF-β1 (3 ng/mL), anti-IFN-γ antibody, anti-IL-4 antibody (both at 20 µg/mL) for 2 days. Cells were subsequently split when necessary using IL-23 (10 ng/mL) containing media for 3 additional days and then plated at 2×10^6 / mL onto plates coated with anti-CD3 / anti-CD28 (both at 2 µg/mL) in the absence of cytokines for 2 days. 5×10^6 cytokine producing cells as assessed on day 2 after initial plating were intravenously injected into C57BL/6 recipients (6–10 weeks old). Animals were sex

matched in transfer experiments. Mice were monitored and assigned grades for clinical signs of EAE using the following scoring system: 0, healthy; 1, limp tail; 2, impaired righting reflex or ataxic gait; 3, hind limb paralysis; 4, total limb paralysis; 5, moribund or death. Mice with a score of >4 were euthanized. If mice died during the course of the experiment, their clinical score of 5 was included in the analysis for the remainder of the experiment.

METHOD DETAILS

Isolation of CNS-Infiltrating Mononuclear Cells

Mice were intracardially perfused with cold PBS. The forebrain and cerebellum were dissected and spinal cords flushed out from the spinal canal with PBS by hydrostatic pressure. CNS tissue was cut into pieces and digested with collagenase D (2.5 mg/mL, Roche Diagnostics) and DNase I (1 mg/mL, Sigma) at 37 °C for 20 min. Mononuclear cells were isolated by passing the tissue through a 70 µm cell strainer, followed by a 70%/37% percoll gradient centrifugation. Mononuclear cells were removed from the interphase, washed and re-suspended in culture medium for further analysis.

CNS Histology

Histological analysis of CNS infiltration was performed as previously described (Jäger et al., 2009). Briefly, mice were sacrificed 28 days after EAE induction or adoptive transfer of T effector cells and brains and spinal cords were fixed in 10% neutral-buffered formalin. Tissues were processed routinely for paraffin embedment and slides were stained with Luxol fast blue-H&E stains. Inflammatory foci (≥ 10 mononuclear cells) were counted in leptomeninges and parenchyma in a blinded fashion.

Enzyme-Linked Immunosorbent Assay

Secreted cytokines were measured after 96h of culture by sandwich enzyme-linked immunosorbent assay (ELISA) as previously described (Jäger et al., 2009). The following antibody clones were used and purchased from Biolegend: IL-17A (TC11-18H10.1), IFN- γ (R4-6A2), IL-17A (TC11-8H4, biotinylated), IFN- γ (XMG1.2, biotinylated).

Flow Cytometry and Related Reagents

For intracellular cytokine staining, cells were stimulated for 4 hr at 37°C with phorbol 12-myristate 13-acetate (PMA, 50 ng/mL; Sigma), ionomycin (1 µg/mL; Sigma) and monensin (GolgiStop; 1 µg/mL; BD Biosciences). After staining for surface markers, cells were fixed and permeabilized according to the manufacturer's instructions (BD Biosciences). FoxP3 staining was performed without PMA and ionomycin and GolgiStop stimulation using FoxP3 staining buffer (eBioscience). Staining phosphorylated STAT proteins for flow cytometry was performed by fixing first with 4% paraformaldehyde, second with 90% methanol at -20°C and then using FoxP3 staining buffer as previously described (Peters et al., 2015). All flow cytometric data were collected on a FACS Calibur or FACS LSR II (both BD Biosciences) and analyzed using FloJo analysis software v7.6.5 (Tree Star). The following antibodies (clone names in brackets) with different fluorochrome labels were purchased from Biolegend: anti-CD4 (RM4-5), anti-CD25 (PC61), anti-CD44 (IM7), anti-CD62L (MEL14), anti-CD90.1 (OX-7), anti-IL-17A (TC11-18H10.1), anti-IFN γ (XMG1.2), anti-IL-5 (TRFK5), anti-CD45.1 (A20), anti-V α 3.2 (RR3-16). The following reagents were purchased from BD and used following the manufacturer's instructions: anti-STAT1 pY701 (4a), anti-STAT3 pY705 (4/P-STAT3), anti-V β 11 (RR3-15), 7AAD, propidium iodide (PI), fluorochrome conjugated Annexin V, Annexin V staining buffer, intracellular cytokine staining kit, Apoptosis Detection Kit (APO-BRDU), Vybrant FAM caspase-8 assay kit. The following antibodies were purchased from eBioscience: anti-Foxp3 (FJK-16s), anti-IL-13 (eBio13A). Inhibitors for caspase 1 (Z-YVAD-FMK), caspase 3 (Z-DEVD-FMK), caspase 8 (Z-IETD-FMK), and of Fas to Fas ligand interaction (Kp7-6) were purchased from EMD Millipore. Kp7-6 was dissolved in H₂O and used at 1mM final concentration.

Isolation and Differentiation of Naive CD4 $^+$ T Cells

CD4 $^+$ CD44 $^{\text{low}}$ CD62L $^{\text{high}}$ CD25 $^-$ naive CD4 $^+$ T cells were purified by FACS sorting following MACS bead isolation of CD4 $^+$ cells. Naive T cells were activated with plate-bound anti-CD3 (2 µg/mL, 145-2C11) and anti-CD28 (2 µg/mL, PV-1) antibody in 96-well (1×10^5 cells/well) or 24-well flat bottom plates. All antibodies for cell culture were provided by the Brigham and Women's Hospital Antibody Core Facility. *In vitro* T cell differentiation was performed for 96 hr. For non-pathogenic Th17 cell differentiation, cultures were supplemented with IL-6 (20 ng/mL) and TGF- β 1 (2 ng/mL). For pathogenic Th17 cells differentiation cultures were supplemented with IL-1 β (20 ng/mL), IL-6 (20 ng/mL) and IL-23 (10 ng/mL). Th1 cell differentiation was performed with IL-12 (20 ng/mL) and anti-IL-4 (11B11; 20 µg/mL). TNF α was used at 20 ng/mL. Differentiation of iTreg cells and Th2 cells were performed with TGF- β 1 (5 ng/mL) and with IL-4 (20 ng/mL), anti-IL-12 (C17.8; 20 µg/mL), respectively. All cytokines were from R&D Systems.

Immunofluorescence Microscopy

CD4 $^+$ CD44 $^{\text{low}}$ CD62L $^{\text{high}}$ CD25 $^-$ sorted naive CD4 $^+$ T cells were incubated on poly-L-lysine slides for 30 min in the presence of IL-6 (20 ng/mL), washed once with PBS, and fixed and permeabilized using Cytofix and Cytoperm (BD Biosciences) for 30 min. Samples were blocked with PBS/5% donkey serum (Abcam) overnight at 4°C and subsequently stained with primary antibodies diluted in PBS/5% donkey serum for 1 hr, followed by three wash steps with PBS. The secondary antibody was diluted in PBS/5% donkey serum and incubated for 1 hr. After additional three wash steps, cells were mounted using DAPI containing mounting medium (CST) and visualized with a confocal laser scanning microscope LSM710 (Zeiss) within 24 hr. All incubations were performed at

room temperature unless indicated otherwise. Antibodies were: rabbit anti-pSTAT1 S727 antibody (clone D3B7, CST, 1:300), FITC conjugated donkey anti-rabbit (Jackson Immuno, 1:1,000), PE-conjugated mouse anti-pSTAT3 Y705 (clone 4/P-STAT3, BD, 1:300). Images were processed and quantified using ImageJ v1.47 (NIH). Five randomly chosen areas of each slide were photodocumented and 12 cells from each photo were randomly picked for analysis in a blinded fashion. For analysis of total protein content, randomly chosen cells were manually outlined and mean fluorescence was measured. For analysis of nuclear phospho-STAT, the nucleus was manually outlined in the DAPI and fluorescence overlay and nuclear fluorescence was quantified in the respective channel. Fluorescence intensity was quantified on a scale from zero (i.e., no intensity) to 255 (i.e., maximum intensity). All slides were processed in parallel and a minimum of 50 cells was analyzed per slide.

Constructs and Luciferase Assays

The pCMV-Stat1 and pCMV-Stat3 vectors containing mouse cDNA sequences were obtained from the PlasmID Repository of Harvard Medical School. The pCMV-Fas construct was generated by PCR amplifying the Fas cDNA from a mouse cDNA library of differentiated Th17 cells from C57BL/6 mice and cloning the fragment into an empty pCMV vector using EcoRI/NotI sites. The coding region was verified by Sanger sequencing. The pGL4-II17a luciferase reporter construct containing 2kb of the mouse *II17a* promoter region was provided by Warren Strober (Addgene plasmid # 20124) (Zhang et al., 2008). The Renilla construct was purchased from Promega.

EL4 cells (5×10^4 cells/well, 96 well flat bottom plate) were cultured in the presence of soluble anti-CD3 and anti-CD28 (each 1 µg/mL) and transiently transfected with Renilla control and pGL4-II17a luciferase vectors using Fugene (Roche). Expression vectors (pCMV-Stat1, pCMV-Stat3, pCMV-Fas) were co-transfected at a range of concentrations (0, 10, 20, 40 ng/mL). Total transfected DNA amount was maintained constant at 125 ng/well by adding empty pCMV vector to substitute for expression vectors. 48 hr after transfection, luminescence was measured with the Dual-Luciferase Reporter Assay System (Promega). The Firefly luciferase activity was normalized to Renilla luciferase activity. Data were normalized between experiments as fold-change versus empty vector control.

RNA Quantification Using nCounter and qPCR Analysis

Gene expression was analysed using the nanostring method as previously described (Lee et al., 2015). Briefly, total RNA extracted using the RNeasy MicroKit (Qiagen) from >50,000 cells was hybridized for 16 hr at 65°C together with the predefined capture and reporter codeset. The samples were then transferred onto the nanostring cartridge using the nCounter prep station. Cartridges were read at maximum resolution. A set of 250 predefined Th17 cell-related transcripts was used (Yosef et al., 2013). Transcripts were only considered if expression was >10 reads and differed >2.0-fold between experimental conditions. Data were calculated as fold regulation of wildtype. Visualization using heatmaps of nanostring data was performed using the GENE-E software. Gene expression was analysed using qPCR by extracting mRNA and reverse transcribing RNA into cDNA using the MultiMACS cDNA Synthesis Kit (Miltenyi) following the manufacturer's instructions. cDNA served as template in TaqMan based qPCR analysis run on a ViiA7 (LifeTechnologies). TaqMan predesigned primer and probe mixes for the indicated transcripts were purchased from Applied Biosystems.

RNA Sequencing

For RNA-seq, total RNA was purified from naïve T cells differentiated in the presence of either no cytokines or TGF-β1 (2 ng/mL) and IL-6 (20 ng/mL) for 48 hr using the RNeasy kit (Qiagen) including DNaseI treatment. Preparation of cDNA libraries for sequencing was performed using the RNA ligation method as previously described (Levin et al., 2010). Briefly, 1 µg of total RNA was polyA-selected twice using oligo-dT beads, then Zinc fragmented, DNase treated, and dephosphorylated. Then 3' RNA-adapter was ligated to the dephosphorylated RNA using T4 RNA Ligase and first strand cDNA synthesis was performed using rTd primers and Affinity Script reverse transcriptase. RNA was then hydrolyzed using NaOH. After clean-up, 5' adapter was ligated to the cDNA and the cDNA was PCR amplified using adapter-complementary primers. Clean-up steps in between reactions were performed using Silane beads. Sequencing was performed on an Illumina HiSeq 2000.

Transcriptional and Gene Set Enrichment Analysis

Differential expression analysis was performed with the Tuxedo Suite. Specifically, we used TopHat (Trapnell et al., 2009) (version 2.0.10), running Bowtie (Langmead and Salzberg, 2012) (version 2.1.0.0) to generate alignments to the mouse genome assembly version 9 (mm9). These were used as input to the Cuffdiff (Trapnell et al., 2010) (version 2.1.1) program for differential expression computations. We used Gene Set Enrichment Analysis (GSEA) to identify gene sets enriched in the RNA-seq data (Subramanian et al., 2005). Specifically, we used the pre-ranked analysis mode, with differentially expressed RNA transcripts ranked by test statistics derived from Cuffdiff. The most significantly over-expressed genes were at the top of the ranked list, while the most under-expressed were at the bottom. We used curated gene sets from pathway databases as available in the Molecular Signature Database (MSigDB) (Subramanian et al., 2005).

Inferred Transcriptional Regulators

We inferred transcriptional regulators responsible for the observed differential pattern of transcription using several approaches. First, we gathered known mouse TFs from the MGI databases (Eppig et al., 2015) (www.informatics.jax.org) using the Gene Ontology term "DNA binding." Then, in the direct approach, we identified all differentially expressed (DE) TFs in our data using FDR assignment

from Cuffdiff (Trapnell et al., 2010). However, TFs causal for differential expression do not have to be differentially expressed themselves at the time point of mRNA expression measurement. Therefore, we searched for differentially expressed genes with binding motifs in their promoters that are associated with known TFs. This was accomplished by first downloading TRANSFAC (Matys et al., 2006)-based TF motifs and corresponding regulated gene lists from MSigDB. Next, using a Kolmogorov-Smirnov (KS) test we assessed the enrichment of each gene list among expressed genes (FPKM > 3) ordered by DE statistic scores. We used a more stringent FDR algorithm (Benjamini and Yekutieli, 2001) for multiple hypothesis testing correction to better address non-independent tests due to overlapping gene lists. In addition, we used the GSEA algorithm (pre-ranked mode) to identify candidate transcriptional regulators in our data using gene modules and their regulators derived from the Ontogenet model, based on ImmGen (www.immgen.org) consortium data.

Protein-Protein Interaction Data and Network Reconstruction

We used a network analysis approach to predict which TFs were most likely affected by Fas given public protein-protein interaction databases and RNA-seq data generated in this study.

We started with a background PPI network collected from the BioGRID (version 3.2.116), HPRD (release 9), and PhosphoSite (2014-09-03) databases. We selected data obtained from human and mouse systems. In BioGRID, we used the following data types: Affinity Capture (except RNA), Biochemical Activity, Co-crystal structure, Co-localization, FRET, Far Western, PCA, Protein-peptide, Proximity Label-MS, Reconstituted Complex, Two-hybrid. From HPRD we used *in vivo* and two-hybrid data. In this study, we were interested in intracellular paths; therefore, we removed secreted proteins (according to UniProt annotations). Overall, we obtained 107,573 interactions across 12,324 proteins.

Next, we noted that network analysis cannot be accomplished trivially by looking up the TFs (DNA-binding proteins) in the network neighborhood of Fas, as there were only 4 of them that were directly connected (*Casp8ap2*, *Trp63*, *Mbd4*, *Rara*), while as many as 191 were connected by at most one intermediate node (Figure 4E) and 766 by two nodes. We therefore ranked the TFs based on the strength of network support for paths connecting them with Fas. We scored those paths based on support by both expression data and better prior knowledge. To assign scores, we noted that protein-protein interaction databases collect interactions that were observed in different cell types (and species), under differing experimental conditions, using various assays, etc. Therefore, a path connecting two proteins is just a possibility that does not have to hold in a specific system being studied. We observe, however, that each additional path linking two proteins increases the chances that the proteins do influence each other. We therefore computed and scored all paths (containing no more than two intermediate nodes) connecting Fas to any other TF in mouse genome. Each path score reflected our approximate belief that path proteins actually participated in carrying the signal between terminal nodes. Thus, the weight of an edge was set to

$$w_e = s \times (1 - (0.25)^n),$$

where n is the number of publications supporting the interaction, 0.25 indicates assumed probability of the interaction being false despite the measurement (59,162 interactions in our network were supported only by two-hybrid or affinity capture MS), and s is an estimate that the interaction takes place in our particular system assuming that interacting proteins are expressed.

We set the node weight as a product of two components $w_n = w_{n1} w_{n2}$. w_{n1} reflected our belief that a given protein was actually expressed in our system and was set to:

$$w_{n1} = 0.05 + 0.95(1 - \exp(-\text{FPKM})),$$

where 0.05 indicates the assumed probability of a protein being expressed despite an observed RNA-seq FPKM equal 0, and the entire formula provides for a rapid increase with increasing FPKM. The second component, w_{n2} reflected the belief that a protein was actively involved in expression changes due to Fas deficiency. For network nodes that were not known to be TFs we used a uniform weight of 0.1. We estimated the chances that a given TF was one of the causal ones for the observed differential expression phenotype in two ways: (1) using enrichments of known DNA-binding motifs and (2) direct measurements of differential expression (described in [Inferred Transcriptional Regulators](#) above). We used minimum FDR from two approaches in the weight computation

$$w_{n2} = 0.5(\text{minFDR}) + 0.1 \text{ minFDR},$$

where 0.5 indicates the assumed probability that the TF node is active when assessed as differentially expressed or having a binding motif associated with DE genes, and 0.1 otherwise (the node weight for Fas was set to 1). We did not distinguish between positively and negatively differentially expressed genes to allow for possible negative regulation. We computed the network path score as a product of node and edge weights (this score ranges between 0 and 1 by definition). The sum of path scores between Fas and a TF reflected the evidence that Fas could influence it. We avoided independently estimating s by separately estimating the influence evidence for paths of specific length. Stat1 had the highest influence score with network paths of having one intermediate node (Figure 4E) and the second highest (after Jun) for paths with two intermediate nodes ([Table S1](#)).

We estimated the statistical significance of influence scores using randomized networks. We shuffled edges between nodes, while preserving node degrees (Maslov and Sneppen, 2002) and also shuffled node weights. We obtained one thousand randomized networks in this way, and in each of them computed influence scores. For each TF we computed the corresponding empirical p value ([Table S1](#)).

Co-immunoprecipitation and Western Blotting

For DISC assembly, 1×10^8 EL4 cells or $5-7 \times 10^7$ MACS sorted primary mouse CD4 $^+$ cells were stimulated for 15 min with either biotinylated anti-Fas antibody (Jo2, 2.5 μ g/mL) and streptavidin (5 μ g/mL, Thermo Scientific) or with multimerized recombinant human Fas ligand (aa 139–281) fused at the N terminus to mouse ACRP30headless (aa 18–111) and a FLAG-tag (MegaFasL, Adipogen) at a final concentration of 100 ng/mL as indicated in the figure legends. MegaFasL was dissolved in H₂O that was used as vehicle. For immunoprecipitation (IP) experiments, cells were then washed twice with ice-cold PBS, lysed in ice-cold IP buffer containing 30 mM Tris HCl, 1% Triton-X100, 150 mM NaCl, 2 mM EDTA, 10% glycerol, 1 mM PMSF, phosphatase inhibitors (HALT, Thermo Scientific) and protease inhibitors (Roche). Immunoprecipitation was performed immediately after lysis using protein G magnetic Dynabeads (Life Technologies) with three consecutive washes with IP buffer. For phosphorylation studies, sorted naive T cells were stimulated with the cytokines as indicated, then washed with PBS, and either lysed in IP buffer or cytoplasmic and nuclear fractions were extracted using NE-PER reagents (Thermo Scientific) following the manufacturer's protocol.

For western blotting, proteins were denatured in the presence of β -mercaptoethanol, separated on pre-cast 4%–12% Bis-Tris SDS-polyacrylamide gels and transferred onto PVDF membranes. Membranes were blocked with 5% non-fat dry milk (Bio-Rad) in TBS-T and primary and HRP coupled secondary antibodies were diluted at 1:1000 in 5% BSA in TBS-T. Detection was performed using ECL substrate (Thermo Scientific) and radiography films. Antibodies for western blotting were purchased from Cell Signaling Technologies: rabbit anti-STAT1, rabbit anti-S727-phospho-STAT1 (D3B7), rabbit anti-Y701-phospho-STAT1 (58D6), rabbit anti-cFlip (D16A8), rabbit anti-Y705-phospho-STAT3 (D3A7), rabbit anti-STAT3 (D3Z2G), rabbit anti-STAT4 (C46B10), mouse anti- β -Actin (8H10D10), rabbit anti-GAPDH (D16H11), rabbit anti-TBP; or Santa Cruz: goat anti-FADD (M19), rabbit anti-FADD (H-181); or EMD Millipore: rat anti-Fas (7C10); or BD: hamster anti-Fas (Jo2). HRP conjugated secondary antibodies against heavy and light chain were: preadsorbed goat anti-rabbit IgG (Abcam), rabbit F(ab')2 Anti-Goat IgG (Southern Biotech), horse anti-mouse IgG (Cell Signaling), goat anti-rat IgG (Santa Cruz).

QUANTIFICATION AND STATISTICAL ANALYSIS

Statistics

Detail regarding the statistical analyses can be found in the figure legends. The term n indicates the number of biological replicates in each experiment (e.g., number of experimental animals). Box-whisker plots or line-whisker plots indicate mean \pm SEM unless indicated otherwise in the figure legend. The percentage of cytokine positive cells in *in vitro* differentiations was compared using Student's t test for paired samples. All other results were analyzed by unpaired Student's t test. p < 0.05 was considered significant. Statistical analysis was performed using GraphPad Prism 5.0.

DATA AND SOFTWARE AVAILABILITY

RNA-sequencing raw data have been deposited in the Gene Expression Omnibus (GEO) under accession number GEO: GSE111244.